Rapidly decorrelating velocity-field model as a tool for solving one-point Fokker-Planck equations for probability density functions of turbulent reactive scalars

Vladimir Sabel'nikov* and Olivier Soulard
ONERA, DEFA/EFCA, Chemin de la Hunière 91761 Palaiseau Cedex, France
(Received 4 August 2004; published 6 July 2005)

Light is shed upon Eulerian Monte Carlo methods and their application to the simulation of turbulent reactive flows. A rapid decorrelating velocity-field model is used to derive stochastic partial differential equations (SPDE's) stochastically equivalent to the modeled one-point joint probability density function of turbulent reactive scalars. Those SPDE's are shown to be hyperbolic, advection-reaction equations. They are dealt with in a generalized sense, so that discontinuities in the scalar fields can be treated. A numerical analysis is proposed and numerical tests are carried out. In particular, a comparison with the Lagrangian Monte Carlo method is performed.

DOI: 10.1103/PhysRevE.72.016301 PACS number(s): 47.27.Eq, 47.70.Fw, 47.11.+j

I. INTRODUCTION

In turbulent flames, phenomena of interest, such as pollutant production, soot formation, or extinctions and ignitions, mainly arise from a conjunction of rare physical events (peak temperature, weak mixing conditions, etc.) and finite-rate chemistry effects. Predicting these phenomena thus requires a precise knowledge of the one-point statistics of the species concentrations and temperature, as well as an accurate description of chemical reactions. Regarding both aspects, the one-point joint composition probability function (PDF) appears as a relevant tool: it transports the detailed one-point statistical information of the turbulent scalars and allows chemical source terms to be treated exactly [1,2].

These advantages are nonetheless counterbalanced by a severe numerical constraint: the composition PDF possesses a potentially high number of dimensions, which induces heavy computational costs. In particular, the finite methods traditionally employed in computational fluid dynamics (CFD) cannot be used, as their cost increases exponentially with dimensionality. Monte Carlo methods, on the other hand, yield a linearly growing effort and are more adapted to solve PDF equations.

So far, in the field of turbulent combustion, Monte Carlo methods have mostly been considered under their Lagrangian form, following the impulsion given by the seminal work of Pope [2]. However, as will be discussed in Sec. VII, Lagrangian Monte Carlo (LMC) methods yield inherent difficulties for controlling statistical convergence and also induce complex couplings with RANS or LES solvers. These results appear as strong incentives to use Eulerian Monte Carlo (EMC) methods. EMC methods are based on stochastic Eulerian fields, which evolve from prescribed stochastic partial differential equations (SPDE's) stochastically equivalent to the PDF equation. In practice, a large set of stochastic fields is evolved and statistics are recovered through weighted sums upon these different realizations. With the notable exception of Valiño's work [3], also discussed in Sec. VII, EMC methods have scarcely been used in the field of turbulent combustion.

In this article, we propose a path to derive SPDE's allowing us to compute a modeled one-point joint composition PDF. This approach has its foundation in the rapidly decorrelating velocity field model first proposed by Kraichnan [4] and Kazantsev [5]. The Kraichnan-Kazantsev (Kr-Ka) model describes the advection of a scalar by a solenoidal white-in-time Gaussian velocity field and leads to a Fokker-Planck composition PDF equation with a diffusion term in physical space. The Kr-Ka model usually serves as a tool for the theoretical analysis of turbulent scalar fields in homogeneous turbulence [6,7].

The Kr-Ka model was used earlier by Eyink and Xin [8] to model nonpremixed isothermal turbulent flames. The starting point of Eyink and Xin [8] is a system of semilinear hyperbolic SPDE's, modeling the evolution of turbulent reactive scalars in the absence of molecular diffusion and in a spatially Lipschitz, incompressible random flow. From this system of SPDE's, Eyink and Xin [8] then derive and analyze closed equations for one-point and multipoint composition PDF's. In this article, we solve, in some sense, an inverse problem. The closed Fokker-Planck equation for the one-point joint composition PDF, as used in the turbulent combustion community [2], is supposed to be given. Contrary to [8], our objective is then to derive SPDE's stochastically equivalent to this given Fokker-Planck equation. In addition, the equivalence between the SPDE's and PDF must now be established for the general case of compressible, inhomogeneous, low-Mach-number turbulent flames, with molecular diffusion effects. It has to be noted that molecular diffusion cannot be neglected for modeling turbulent reactive flows. In fact, combustion can only occur after molecular mixing has taken place.

The SPDE's that we derive are semilinear hyperbolic equations, advected by a smooth in space, white-in-time velocity field. Spatial smoothness of the velocity field proceeds from the fact that the impact of a white-in-time velocity field on the one-point composition PDF is characterized only by the turbulent diffusivity tensor [6,7]. Further details of the spatial structure of a white-in-time velocity field do not influence this one-point composition PDF (this is not the case for multipoint PDF's [6,8]). As the turbulent diffusivity tensor is spatially Lipschitz, the stochastic velocity that we derive is also spatially Lipschitz. This fact essentially simplifies

*Electronic address: Vladimir.Sabelnikov@onera.fr

the derivation and proof of the equivalence between the SPDE's and PDF.

In the derived SPDE's, the stochastic advection term is interpreted in the Stratonovitch sense: as will be shown, only in this case can the SPDE's be considered as advection-reaction equations. These SPDE's are also treated in a generalized sense. Indeed, discontinuous stochastic scalar fields are likely to appear due to the influence of boundary conditions, even for continuous and differentiable initial solutions. Finally, due to their hyperbolicity, the SPDE's are shown to be intimately connected to Lagrangian methods through the notion of stochastic characteristic.

The remainder of the paper is organized as follows. First, a modeled equation for the composition one-point PDF is given. Then, SPDE's allowing one to compute this PDF are derived. The connection of these SPDE's with stochastic ordinary differential equations (SODE's) is precised through the notion of stochastic characteristics. A simple example is proposed to illustrate this connection, as well as the basic features of the SPDE's. Then, a numerical analysis is carried out and numerical tests are performed to check orders of accuracy and statistical convergence rates. Finally, a discussion of the relative merits of the LMC and EMC approaches is proposed.

II. PDF EQUATION OF A TURBULENT REACTIVE SCALAR

Without loss of generality, the one-point composition PDF—and the subsequent derivation of the SPDE's allowing to compute it—is detailed for only one turbulent reactive scalar c. This scalar evolves according to an advection-diffusion-reaction equation

$$\frac{\partial c}{\partial t} + U_j \frac{\partial c}{\partial x_j} = -\frac{1}{\rho}\frac{\partial J_j}{\partial x_j} + S(c). \tag{1}$$

The left-hand side describes the advection of the scalar field by the turbulent velocity $\boldsymbol{U}$ while the two terms on the right-hand side, respectively, describe the effects of molecular diffusion and chemical reaction: J_j represents the molecular diffusion flux and $S(c)$ is a chemical source term, depending on the scalar value.

For variable density flows with low Mach numbers, working with density-weighted (Favre) statistics is a widespread technique. If p_c is the one-point PDF of the scalar c, then the Favre one-point PDF f_c is defined by

$$\langle\rho\rangle f_c(c;\boldsymbol{x},t) = \rho(c)p_c(c;\boldsymbol{x},t), \tag{2}$$

where ρ is the density. The Reynolds average of a quantity Q is noted $\langle Q\rangle$. Its Favre average and Favre fluctuation are, respectively, denoted $\widetilde{Q}$ and $Q''=Q-\widetilde{Q}$. From the definition of the Favre PDF [Eq. (2)], we have the well-known relation $\widetilde{Q}=\langle\rho Q\rangle/\langle\rho\rangle$

The low-Mach-number assumption is here necessary for expressing the density as a function of the scalar concentration $\rho=\rho(c)$. In this work, it will be supposed that this assumption is verified.

Using standard techniques [2], the following transport equation is obtained for the Favre PDF f_c:

$$\begin{aligned}\frac{\partial}{\partial t}(\langle\rho\rangle f_c) + \frac{\partial}{\partial x_j}(\langle\rho\rangle \widetilde{U}_j f_c) &= -\frac{\partial}{\partial x_j}(\langle\rho\rangle\langle u_j''|c\rangle f_c) \\ &\quad - \frac{\partial}{\partial c}\left(\langle\rho\rangle\left\langle -\frac{1}{\rho}\frac{\partial J_j}{\partial x_j}|c\right\rangle f_c\right) \\ &\quad - \frac{\partial}{\partial c}[\langle\rho\rangle S(c) f_c],\end{aligned} \tag{3}$$

where $\langle\cdot|c\rangle$ denotes averages conditioned on the scalar value.

The left-hand side of this equation represents the advection of f_c by the Favre-averaged velocity $\widetilde{U}$. The first term on the right-hand side describes the effects of turbulent advection by the fluctuating velocity $\boldsymbol{u''}=\boldsymbol{U}-\widetilde{\boldsymbol{U}}$, the second the effects of molecular mixing, and the third the effects of chemical reaction. While chemical reactions are treated exactly, the effects of molecular mixing, and turbulent advection appear in an unclosed form and require modeling.

The conditional average of the divergence of the scalar flux, $\langle -(1/\rho)\partial J_j/\partial x_j|c\rangle$, is usually called the micromixing term and in the general case is modeled by an operator noted $\mathcal{M}$. Two of the most frequently used models, which will be considered in this work, are the IEM model [9]

$$\mathcal{M}f_c = -\langle\omega_c\rangle(c-\widetilde{c})f_c \tag{4}$$

and the Langevin model [10,11]

$$\mathcal{M}f_c = -a\langle\omega_c\rangle(c-\widetilde{c})f_c - \frac{\partial}{\partial c}[b\langle\omega_c\rangle c(1-c)f_c],$$

$$a = 1 + d_0\frac{\widetilde{c}-\widetilde{c^2}}{\sigma_M^2}, \quad b = d_0\frac{\sigma^2}{\sigma_M^2}. \tag{5}$$

In these equations, σ^2 is the scalar variance,

$$\sigma^2 = \widetilde{c_2} - \widetilde{c}^2, \tag{6}$$

and σ_M^2 is the maximum value of the scalar variance:

$$\sigma_M^2 = \widetilde{c}(1-\widetilde{c}), \tag{7}$$

$\langle\omega_c\rangle$ is the mean mixing frequency and d_0 is a positive constant controlling the rate of PDF relaxation. If $d_0=0$, then the Langevin model transforms into the IEM model.

The IEM and Langevin models can be considered as variants of the mean-field approximation, since the two-point statistical information needed for $\langle -(1/\rho)\partial J_j/\partial x_j|\mathcal{C}\rangle$ is modeled using the one-point PDF and its first moments $(\widetilde{c},\widetilde{c^2})$. The explicit formulation of the IEM and Langevin models will only be used in the applications and the general form $\mathcal{M}$ will be kept unless explicitly noted otherwise.

As for turbulent advection, it is usually modeled with an isotropic gradient diffusion assumption [2]:

$$\langle u_j''|c\rangle f_c = -\Gamma_T\frac{\partial f_c}{\partial x_j}, \tag{8}$$

where Γ_T is a turbulent diffusion coefficient.

As a result, the following modeled transport equation is obtained for f_c, the Favre one-point PDF of c:

$$\frac{\partial}{\partial t}(\langle\rho\rangle f_c) + \frac{\partial}{\partial x_j}(\langle\rho\rangle \widetilde{U}_j f_c) = \frac{\partial}{\partial x_j}\left(\langle\rho\rangle \Gamma_T \frac{\partial f_c}{\partial x_j}\right) - \frac{\partial}{\partial c}(\langle\rho\rangle \mathcal{M} f_c) - \frac{\partial}{\partial c}[\langle\rho\rangle S(c) f_c]. \quad (9)$$

In this equation, the turbulent diffusivity Γ_T and the mean mixing frequency $\langle\omega_c\rangle$, as well as the Favre-averaged velocity $\widetilde{\boldsymbol{U}}$, are supposed to be known. For instance, they can be computed from a RANS solver [12]. As a consequence, this equation is closed. Note that if $\mathcal{M}f_c$ does not include derivatives in composition space (as with the IEM model), Eq. (9) is parabolic in space and hyperbolic in composition space, so that it is a degenerate hypoelliptic Fokker-Planck equation.

We note here that the PDF equation derived in [8] corresponds to a particular case of Eq. (9), with constant density ρ, zero mean advection $\widetilde{\boldsymbol{U}}=0$, constant turbulent diffusion Γ_T, and no micromixing $\mathcal{M}=0$.

III. DERIVATION OF THE SPDE's

Our main objective here is to derive an SPDE stochastically equivalent to the PDF equation (9). This SPDE governs the evolution of a stochastic scalar field hereafter denoted θ.

In devising such an SPDE, the major difficulty does not stem from the influence of mean advection, chemical reactions, or micromixing. Mean advection and chemical reactions appear under an exact form in the PDF equation (9) and will also be present under an exact form in the stochastic field equation. As for micromixing, a stochastic process yielding an operator $\mathcal{M}$ in the PDF equation (9) has already been devised in the frame of LMC methods and can be readily applied to our case (see Appendix A). This process is further denoted $M(\theta;x,t)$ and is added as a source term in the stochastic field equation. For the IEM model, M is deterministic and is defined by [9]

$$M(\theta;x,t) = -\langle\omega_c\rangle(\theta - \widetilde{\theta}). \quad (10)$$

For the Langevin model, M is stochastic and is defined by [10,11]

$$M(\theta;x,t) = -a\langle\omega_c\rangle(\theta - \widetilde{\theta}) + \sqrt{2b\langle\omega_c\rangle\theta(1-\theta)}\,\dot{W}, \quad (11)$$

where $W(t)$ is a standard Wiener process and $\dot{W}$ is its time derivative (white noise). In this expression, the stochastic product is interpreted with the Ito interpretation (see [13] and below for further information on the Ito interpretation). The absence of symbol in the stochastic product denotes this interpretation.

The last and main question that now remains to be answered is how to model the turbulent advection in the scalar field SPDE, so as to get the diffusion term in the PDF equation.

To try and figure out this problem, the equation for the stochastic field θ is first written in the following form:

$$\frac{\partial\theta}{\partial t} + u_j\frac{\partial\theta}{\partial x_j} = F(\theta;x,t), \quad (12)$$

where $F(\theta;x,t) = -\widetilde{U}_j\,\partial\theta/\partial x_j + M(\theta;x,t) + S(\theta)$ accounts for mean advection, micromixing, and chemical reaction as explained above. In Eq. (12), $\boldsymbol{u}$ is a stochastic velocity which needs to be specified. It does not directly correspond to the Favre fluctuating velocity $\boldsymbol{u}''$ and in particular does not necessarily respect the continuity constraint and does not necessarily average to zero. Only two features are of interest for our purpose. The first one is that $\boldsymbol{u}$ models a velocity and thus should preserve the physical property of advection. The second one is that $\boldsymbol{u}$ should yield, in the one-point PDF equation derived from Eq. (12), the diffusion term present in Eq. (9).

Concerning this second point, it is known, from the works of Kraichnan [4] and Kazantsev [5] or from those of Eyink and Xin [8], that a diffusion term in the PDF equation can be obtained with a white-in-time Gaussian velocity field. However, these results were obtained under the assumption of a homogeneous and solenoidal stochastic velocity field. In our case, the gradient diffusion coefficient is variable in space, and, besides, the density is variable. Consequently, the assumption of homogeneous and solenoidal stochastic velocity fields is not valid: we need to modify the Kr-Ka model to account for the specificities of our case.

In addition, we also consider the use of the Kr-Ka model from a different angle, compared to [4,5,8]. Our goal is to compute one-point PDF's, so that, as will be shown, we only need to know the turbulent diffusion coefficient. The details of the spatial structure of the white-in-time Gaussian velocity field are of no importance to our purpose, as opposed to [4,5,8].

The key idea of our approach consists in modeling $\boldsymbol{u}$ as

$$\boldsymbol{u} = \boldsymbol{u}^d + \boldsymbol{u}^g, \quad (13)$$

where $\boldsymbol{u}^d$ is a deterministic drift component and $\boldsymbol{u}^g$ is a Gaussian random component of the velocity. Then, in Eq. (12), we let the correlation time of $\boldsymbol{u}^g$ tend to zero. When taking this zero-correlation time limit, several limit equations with different interpretations (Ito, Stratonovitch, etc.) can be obtained (see [13] for more details on Ito and Stratonovitch interpretations). However, only one limit equation preserves the physical property of advection: the one that is obtained in the same way Stratonovitch did to give meaning to his stochastic integral [13].

As a result, we obtain the following SPDE with Stratonovitch interpretation for the stochastic advection term:

$$\frac{\partial\theta}{\partial t} + u_j^d\frac{\partial\theta}{\partial x_j} + u_j^g \circ \frac{\partial\theta}{\partial x_j} = F(\theta,x). \quad (14)$$

The symbol $\circ$ is used to denote the Stratonovitch interpretation of the stochastic product. The velocity $\boldsymbol{u}^g$ is now δ correlated in time.

It is essential to note that this equation is a hyperbolic advection-reaction equation. The Stratonovitch calculus is identical to the classical one, so that $u_j^g \circ \partial\theta/\partial x_j$ has the same physical advection properties as if $\boldsymbol{u}^g$ was deterministic. In

particular, if $M=0$ and $S=0$, then the stochastic field θ is simply advected alongside a stochastic path. Except for the influence of boundary conditions, initial profiles are strictly preserved and do not undergo any kind of diffusion process. This advection properties would be lost if an Ito interpretation was used (see Sec. V).

The last step in the derivation of an equation for the stochastic field consists in precising $\boldsymbol{u}^d$ and $\boldsymbol{u}^g$ so that the PDF of θ is identical to f_c. This can be achieved by expressing the PDF equation of the stochastic scalar field θ and by identifying it with the PDF equation (9) of c. This procedure is detailed in Appendix A and yields the following constraints on $\boldsymbol{u}^d$ and $\boldsymbol{u}^g$:

$$\frac{1}{2}\langle u_i^g(x,t)u_j^g(x,t)\rangle dt = \Gamma_T \delta_{ij}, \tag{15}$$

$$u_j^d = -\frac{1}{2}\left\langle \frac{\partial u_i^g}{\partial x_i}(x,t)u_j^g(x,t)\right\rangle dt - \frac{1}{\langle\rho\rangle}\frac{\partial\langle\rho\rangle}{\partial x_j}\Gamma_T. \tag{16}$$

The constraint equations (15) and (16) do not determine uniquely the velocities $\boldsymbol{u}^d$ and $\boldsymbol{u}^g$. Concerning the first constraint (15), our choice is to use the simplest possible solution—i.e., an isotropic stochastic velocity:

$$u_j^g = \sqrt{2\Gamma_T}\dot{W}_j, \tag{17}$$

where the W_j are independent standard Brownian processes and the $\dot{W}_j$ are their time derivatives. The Brownian processes W_j are also chosen independent from the Brownian process W used in the Langevin model. From this expression and from the constraint equation (16), we deduce, for the drift velocity,

$$u_j^d = -\frac{1}{2}\frac{\partial\Gamma_T}{\partial x_j} - \frac{1}{\langle\rho\rangle}\frac{\partial\langle\rho\rangle}{\partial x_j}\Gamma_T. \tag{18}$$

We emphasize that the stochastic velocity field $\boldsymbol{u}^g$ is only dependent on the turbulent diffusivity Γ_T. As Γ_T is Lipschitz continuous in space, the stochastic velocity field is also Lipschitz continuous in space. This conclusion is essential for the derivation presented in Appendix A.

Finally, the following SPDE is obtained:

$$\frac{\partial\theta}{\partial t} + \left(\tilde{U}_j - \frac{1}{2}\frac{\partial\Gamma_T}{\partial x_j} - \frac{1}{\langle\rho\rangle}\frac{\partial\langle\rho\rangle}{\partial x_j}\Gamma_T\right)\frac{\partial\theta}{\partial x_j} + \sqrt{2\Gamma_T}\dot{W}_j \circ \frac{\partial\theta}{\partial x_j} = M(\theta;x,t) + S(\theta). \tag{19}$$

This equation is a hyperbolic advection-reaction equation, stochastically equivalent to the PDF equation (9). In its derivation, no hypothesis on the smoothness and differentiability of the stochastic scalar fields was required so that it has a generalized sense. Besides, the velocity advecting the stochastic field is formed by mean quantities, so that its length scale is also that of a mean quantity. This, however, does not imply that the scalar field also evolves on a mean length scale. Equation (19) is also driven by a chemical source term which, in practice, possesses stiff gradients in composition space. These in turn can generate strong gradients in physical space for the stochastic fields (see example in Sec. V C).

The stochastic advection term in Eq. (19) is expressed with a Stratonovitch interpretation. It can also be recast with an Ito interpretation [13] (see Appendix B):

$$\frac{\partial\theta}{\partial t} + \tilde{U}_j\frac{\partial\theta}{\partial x_j} + \sqrt{2\Gamma_T}\dot{W}_j\frac{\partial\theta}{\partial x_j} - \frac{1}{\langle\rho\rangle}\frac{\partial}{\partial x_j}\left(\langle\rho\rangle\Gamma_T\frac{\partial\theta}{\partial x_j}\right) = M(\theta;x,t) + S(\theta). \tag{20}$$

This equation was first found by Valiño [3], but under a restrictive hypothesis on the smoothness of the scalar field (see Sec. VII). It was also considered in [3] as a parabolic SPDE. As will be clarified in Sec. V, the presence of a second-order spatial operator in Eq. (20) is deceptive. Because of the stochastic term with Ito interpretation, it does not act as a diffusion term but, instead, contributes with the stochastic term to the advection of the scalar field. As Eq. (19), Eq. (20) is an advection-reaction equation. For instance, in the case of no molecular mixing or chemical reaction, the scalar θ is constant alongside Brownian paths.

IV. STOCHASTIC CHARACTERISTICS: A BRIDGE BETWEEN LAGRANGIAN AND EULERIAN MONTE CARLO METHODS

In Sec. III, an SPDE [Eq. (19)] stochastically equivalent to the Fokker-Planck PDF equation (9) has been derived. This SPDE can be solved as such to compute the evolution of a large set of Eulerian stochastic fields, from which the PDF (9) is eventually reconstructed. This procedure yields, by definition, a Eulerian Monte Carlo method.

There also exists another way of exploiting Eq. (19). Indeed, as shown in Sec. III, SPDE (19) is a first-order hyperbolic equation. Therefore, it possesses characteristic curves along which it reduces to an SODE (compatibility equation) [14]. As a result, Eq. (19) can also be solved by the method of characteristics—that is to say, by solving the set of SODE's defining its characteristic curves and its compatibility equation. This procedure yields, in turn, a Lagrangian Monte Carlo method, different from the one introduced in [2] (see Sec. IV B).

A. Notion of a stochastic characteristic

The correspondence between characteristics and hyperbolic equations is straightforward for deterministic PDE's, and it can also be intuitively extended to hyperbolic SPDE's as long as they involve velocities with nonzero correlation times. However, for SPDE's with white-in-time velocities, as in our case, the notion of characteristic needs to be precised.

SPDE (19) has been derived in Sec. III by considering the zero-correlation time limit in the Stratonovitch sense of the stochastic advection term in Eq. (12). With all its term expanded, Eq. (12) can be rewritten as

$$\frac{\partial\theta}{\partial t} + \tilde{U}_j\frac{\partial\theta}{\partial x_j} + u_j\frac{\partial\theta}{\partial x_j} = M(\theta;x,t) + S(\theta). \tag{21}$$

In Eq. (21), the zero-correlation time limit of the random velocity $\boldsymbol{u}$ is not yet taken. As a result, Eq. (21) is equivalent to the following characteristic system:

$$d\theta^+(t) = [M(\theta^+(t);\boldsymbol{x}^+(t),t) + S(\theta^+(t))]dt, \tag{22}$$

$$dx_j^+(t) = \tilde{U}_j dt + u_j dt. \tag{23}$$

The notation $q^+(t)$ is hereafter used to denote the value of a quantity q taken along the characteristic path $\boldsymbol{x}^+(t)$. For instance, we write $\theta^+(t)$ for $\theta(t,\boldsymbol{x}^+(t))$. Provided that initial and boundary conditions are the same, both SPDE (21) and SODE's (22) and (23) share the same solution Θ_τ, where the subscript denotes the dependence of the solution on τ, the correlation time of $\boldsymbol{u}$.

When τ tends to zero with respect to other characteristic time scales, several limit equations with different interpretations (Ito, Stratonovitch, etc.) can be obtained, respectively, from SPDE (21) and from SODE's (22) and (23). Then, the limit SPDE and the limit set of SODE's do not necessarily possess the same solution and cannot *a priori* be considered as equivalent.

However, in the Stratonovitch sense, the limit SPDE of Eq. (21) can schematically be defined as the limit equation which solution is Θ_0—i.e., the limit when $\tau \to 0$ of Θ_τ. As Θ_τ and thus Θ_0 are the same for Eqs. (22) and (23), this definition also holds for the limit SODE's obtained from Eqs. (22) and (23), in the Stratonovitch sense.

As a consequence, the zero-correlation time limits in the Stratonovitch sense of SPDE (21) and SODE's (22) and (23) are equivalent: both limit equations share the same solution Θ_0. Thus, the notion of a characteristic can also be extended intuitively to the case of hyperbolic SPDE's with white-in-time velocities, provided that the Stratonovitch interpretation is used in both the SPDE and its characteristics.

We recall here that this discussion deals with the zero-correlation time limit of the advection process and is independent of the specification of the micromixing model. By construction, the Langevin model (11) uses the Ito interpretation, and this interpretation is kept on the right-hand side of the hyperbolic SPDE and in its compatibility equation.

In particular, the characteristics of SPDE (19) are given by

$$d\theta^+(t) = [M(\theta^+(t);x,t) + S(\theta^+(t))]dt, \tag{24}$$

$$dx_j^+(t) = \left(\tilde{U}_j - \frac{1}{2}\frac{\partial \Gamma_T}{\partial x_j} - \frac{1}{\langle\rho\rangle}\frac{\partial\langle\rho\rangle}{\partial x_j}\Gamma_T\right)dt + \sqrt{2\Gamma_T} \circ dW_j(t). \tag{25}$$

SODE's (24) and (25) can be viewed as describing the Lagrangian trajectories of stochastic particles in physical and composition space. They can serve as a basis to compute the Lagrangian statistics of the scalar field θ.

SODE (25) with Stratonovitch interpretation can be recast in an SODE with Ito interpretation. System (24) and (25) then becomes

$$d\theta^+(t) = [M(\theta^+(t);x,t) + S(\theta^+(t))]dt, \tag{26}$$

$$dx_j^+(t) = \left(\tilde{U}_j - \frac{1}{\langle\rho\rangle}\frac{\partial\langle\rho\rangle}{\partial x_j}\Gamma_T\right)dt + \sqrt{2\Gamma_T}\, dW_j(t). \tag{27}$$

As opposed to SODE's (24) and (25) and SPDE (19) with Stratonovitch interpretation, there is no direct connection between SODE's (26) and (27) and (20) with Ito interpretation: SODE's (26) and (27) cannot be viewed as characteristics of the "parabolic" SPDE (20).

B. Correspondence between Lagrangian and Eulerian descriptions

SODE's (24) and (25) are equivalent to SPDE (19), but yield a purely Lagrangian description of the statistics of the scalar field θ. If one is interested in computing Eulerian statistics, a supplementary information must be introduced.

In a Lagrangian framework, the evolution of the stochastic field is computed along the trajectories of a set of particles. Each trajectory is characterized by the initial particle position, denoted $\boldsymbol{x}^+(0) = \boldsymbol{\xi}$, so that the computed positions and scalar values are functional of ξ: $\boldsymbol{x}^+(t) = \boldsymbol{x}^+(t|\boldsymbol{\xi})$ and $\theta^+(t) = \theta^+(t|\boldsymbol{\xi})$. A Eulerian description, on the other hand, requires the scalar values carried by the particles to be explicitly known as functionals of the current particle positions. Thus, to make the Lagrangian-Eulerian connection complete, one needs to know how to transform the initial positions of the particles to their current positions or, in other words, to express $\boldsymbol{\xi}$ as $\boldsymbol{\xi}(x^+)$. This transformation is given by the Jacobian $j^+(t|\boldsymbol{\xi})$ of the current position $x^+(t)$ of the stochastic particles with respect to there initial position:

$$j^+(t|\boldsymbol{\xi}) = \mathrm{Det}[j_{ik}(t|\boldsymbol{\xi})], \tag{28}$$

with

$$j_{ik} = \frac{\partial x_i^+(t|\boldsymbol{\xi})}{\partial \xi_k}.$$

As shown in Appendix C, the relation between the Eulerian PDF of θ, $f_E(\Theta;x,t)$, and the Lagrangian joint PDF of $\theta(t|\xi)$ and particle position $\boldsymbol{x}(t|\xi)$, $f_L(\Theta,x;t|\xi)$ is given by

$$\int f_L(\Theta,x;t|\xi)d\xi = \left\langle \frac{1}{j}|\Theta \right\rangle f_E(\Theta;x,t). \tag{29}$$

Thus, to recover the Eulerian PDF from a set of Lagrangian stochastic particles, it is necessary to know the Jacobian j^+. Except for the particular case of particles advected by an isovolume (divergence-free) velocity field, for which the Jacobian is equal to 1, the evolution of j^+ is not trivial. For Eq. (25), this evolution is given by

$$dj^+ = j^+ div(\tilde{\boldsymbol{U}} + \boldsymbol{u}^d + \boldsymbol{u}^g)dt = j^+\left[\frac{\partial}{\partial x_k}\left(\tilde{U}_k - \frac{1}{2}\frac{\partial \Gamma_T}{\partial x_k} - \frac{1}{\langle\rho\rangle}\frac{\partial\langle\rho\rangle}{\partial x_k}\Gamma_T\right)dt + \frac{\partial}{\partial x_k}(\sqrt{2\Gamma_T}) \circ dW_k\right]. \tag{30}$$

$\boldsymbol{u}^d$ and $\boldsymbol{u}^g$ are synthetic velocity fields and their divergences are not linked with the evolution of density. For instance, even in the case of constant density, $\mathrm{div}(\tilde{\boldsymbol{u}} + \boldsymbol{u}^d + \boldsymbol{u}^g)$ is not zero, so that j^+ cannot be taken equal to 1. As a consequence,

in the general case, no simplification can be brought to Eq. (30). It is thus necessary to solve Eq. (30) alongside with SODE's (24) and (25) in order to compute the Eulerian PDF (9).

The Lagrangian approach described here differs from the traditional one introduced in [2]. This last approach can be viewed as a finite pointset method [15] discretizing a stochastic Eulerian PDF equation written in a conservative form, and equivalent to Eq. (9). The solution of the stochastically equivalent PDF equation is looked for in the following form:

$$\langle\rho\rangle\bar{f}_{N_p}(c;x,t) = \Delta m \sum_{k=1}^{N_p} \delta(\bar{x}_k(t) - x)\,\delta(\bar{c}_k(t) - c), \qquad (31)$$

where N_p is a number of stochastic particles and Δm is a mass carried by each particle. Then, by introducing this expression into Eq. (9) and after several manipulations, one obtains the SODE's with Ito interpretation [2]:

$$d\bar{c}(t) = [M(\bar{c}(t);\bar{x}(t),t) + S(\bar{c}(t))]dt, \qquad (32)$$

$$d\bar{x}_j(t) = \left(\tilde{U}_j + \frac{1}{\langle\rho\rangle}\frac{\partial\langle\rho\rangle\Gamma_T}{\partial x_j}\right)dt + \sqrt{2\Gamma_T}\,dW_j(t). \qquad (33)$$

The main advantage of this description is that it avoids introducing an equation for the Jacobian. However, the notion of stochastic characteristic is lost. SODE's (32) and (33) cannot be interpreted any longer as defining the trajectories of Lagrangian particles having statistics equivalent to the PDF (9). We note in particular that SODE's (32) and (33) are also different from SODE's (26) and (27) obtained through the notion of stochastic characteristic.

V. ILLUSTRATION OF THE PROPERTIES OF HYPERBOLIC ADVECTION-REACTION SPDE's

The purpose of this section is to try and clarify some of the properties of the hyperbolic advection-reaction equation (19). To this end, the following simplifications are introduced: a one-dimensional domain is considered and the density ρ is chosen constant, as well as the turbulent diffusion coefficient $\Gamma_T = \Gamma$. The corresponding abridged version of Eq. (9) is then given by

$$\frac{\partial f_c}{\partial t} = \Gamma\frac{\partial^2 f_c}{\partial x^2} - \frac{\partial}{\partial c}[\mathcal{M}f_c + S(c)f_c]. \qquad (34)$$

Four different aspects of Eq. (19) are illustrated. The first example aims at gaining more insight into the connection between PDF equations and hyperbolic SPDE's and, more generally, at illustrating the advecting properties of hyperbolic SPDE's. The second case discovers the impact of boundary conditions on the regularity of the solutions of hyperbolic SPDE's. In the third example, the influence of a stiff chemical source term is illustrated. Finally, the last example describes the effects of micromixing on the regularity of the solutions of hyperbolic SPDE's.

In the first two cases, only pure turbulent advection is involved; i.e., there is no micromixing or reaction: $\mathcal{M}=0$ and $S(c)=0$, so that Eq. (34) degenerates further to a diffusion equation

$$\frac{\partial f_c}{\partial t} = \Gamma\frac{\partial^2 f_c}{\partial x^2}. \qquad (35)$$

In the first case, the physical domain is chosen unbounded, while in the second, a finite domain is considered. In the third case, micromixing is not included $\mathcal{M}=0$, and a discontinuous source term is introduced. This term aims at reproducing the strong gradients of Arrhenius chemical source terms in the case of extremely high activation energies. It is defined by

$$S_a(c) = \begin{cases} \varepsilon S_M, & \text{if } 0 \leqslant c < c_a, \\ S_M, & \text{if } c_a \leqslant c < 1, \\ 0 & \text{else}, \end{cases} \qquad (36)$$

where S_M, ε, and c_a are constants and $\varepsilon \ll 1$. Finally, in the fourth example, the IEM micromixing model [Eq. (10)] is considered, with a constant mixing frequency $\langle\omega_c\rangle = \omega$.

A. Pure turbulent advection, unbounded domain: Advecting properties of hyperbolic SPDE's

1. PDF equation and hyperbolic SPDE's

In this section, a direct connection between PDF (35) and an hyperbolic SPDE is exhibited. Let the initial condition of Eq. (35) be given by

$$f(c;x,t=0) = f_0(c;x). \qquad (37)$$

The solution of the parabolic equation (35) is then

$$f(c;x,t) = \int f_0(c;x-y)\frac{1}{\sqrt{4\pi\Gamma t}}e^{-y^2/4\Gamma t}dy. \qquad (38)$$

By definition, the function $(1/\sqrt{4\pi\Gamma t})e^{-y^2/4\Gamma t}$ is the PDF of the Brownian process $y=\sqrt{2\Gamma}W$ (W is the standard Brownian process). Hence, the integral on the right-hand side of Eq. (38) can be interpreted as the mean of $f_0(c;x-\sqrt{2\Gamma}W(t))$:

$$f(c;x,t) = \langle f_0(c;x - \sqrt{2\Gamma}W)\rangle_W, \qquad (39)$$

where $\langle\cdot\rangle_W$ denotes averaging over the Brownian process. Now, one can identify the function $\hat{f}(c;x,t)=f_0(c;x - \sqrt{2\Gamma}W(t))$ as a first integral of the first-order SODE's:

$$dc = 0,$$

$$dx = \sqrt{2\Gamma}dW(t). \qquad (40)$$

The term "first integral" means that $\hat{f}$ is constant alongside the trajectory given by the SODE's (40). As a result, knowing the initial condition f_0 and the trajectories given by Eqs. (40) allows one to compute the PDF f through Eq. (39).

In the deterministic case, ODE's similar to Eqs. (40) are named characteristic curves of hyperbolic advection PDE's. In the stochastic case, it is logical to name the SODE's (40) stochastic characteristic curves of the following hyperbolic advection SPDE:

$$\frac{\partial c}{\partial t}dt + \sqrt{2\Gamma}\frac{\partial c}{\partial x} \circ dW = 0. \tag{41}$$

Equation (41) is the abridged version of Eq. (19). As was stated above, it describes the pure turbulent stochastic advection of the concentration field by the white in time velocity field $\sqrt{2\Gamma}dW$.

The Stratonovitch interpretation, as explained in Sec. III, arises from considering a limit of a short correlated velocity field. This interpretation is essential: if one erroneously chooses the Ito interpretation, then one gets, after averaging Eq. (41) with Ito interpretation,

$$\frac{\partial \langle c \rangle}{\partial t} = 0, \tag{42}$$

since for the Ito interpretation $\langle \sqrt{2\Gamma}(\partial c/\partial x)\, dW \rangle = 0$. This result is incompatible with the scalar mean equation deduced from the PDF equation (35):

$$\frac{\partial \langle c \rangle}{\partial t} = \Gamma \frac{\partial^2 \langle c \rangle}{\partial x^2}. \tag{43}$$

With the Stratonovitch interpretation, this correlation is not zero. Indeed, the Furutsu-Novikov formula [13] gives, for the stochastic product,

$$\left\langle \sqrt{2\Gamma}\frac{\partial c}{\partial x} \circ dW \right\rangle = -\Gamma \frac{\partial^2 \langle c \rangle}{\partial x^2}. \tag{44}$$

This in turn is compatible with the equation of the averaged scalar Eq. (43).

Equation (41) can be rewritten in Ito form, which corresponds to the abridged version of Eq. (20):

$$\frac{\partial c}{\partial t}dt + \sqrt{2\Gamma}\frac{\partial c}{\partial x}\, dW - \Gamma \frac{\partial^2 c}{\partial x^2}dt = 0. \tag{45}$$

This equation is a particular case of Eq. (B5) for Γ constant.

A simple—nonrigorous—way to understand the Ito transformation is to add a deterministic term to the stochastic advection term with Stratonovitch interpretation so that it yields a zero correlation. The mean of the stochastic product with Stratonovitch interpretation is given by the Furutsu-Novikov formula (44). By subtracting a diffusion term to the Stratonovitch interpretation, one naturally obtains a stochastic term with Ito interpretation:

$$\sqrt{2\Gamma}\frac{\partial c}{\partial x}\, dW = \sqrt{2\Gamma}\frac{\partial c}{\partial x} \circ dW - \Gamma \frac{\partial^2 c}{\partial x^2}dt. \tag{46}$$

A more formal proof is given in Appendix B.

2. Advecting properties of SPDE's (41) and (45)

The Stratonovitch interpretation preserves the classical differential calculus [13], so that Eq. (41) is an hyperbolic advection equation as would be the case if the coefficient in the advection term had a nonzero correlation time. The solution of Eq. (41) is thus simply given by

$$c(x,t) = c_0(x - \sqrt{2\Gamma}W(t)), \tag{47}$$

where c_0 is the initial condition of the stochastic field c. Equation (47) is another way of expressing the fact that Eq. (41) preserves the shape of the initial solution and advects it along Brownian paths. In particular, even an initial discontinuous profile such as the Heaviside function $H(x)$ is transported without alteration.

This advecting property might seem paradoxical when considering that Eq. (41) is equivalent to Eq. (45) with Ito interpretation. Equation (45) has a second-order diffusion term, so that it looks like a parabolic equation. However, the term with Brownian noise is not an advection term, because the Ito calculus does not have the same rules as the classical differential calculus. In this case, as already mentioned, it is the sum of the Brownian noise term and of the diffusionlike term which is meaningful and which acts like an advection term. And one can verify by direct use of the Ito formula [13] that Eq. (47) is also a solution of Eq. (45).

It can also be checked that the solution (47) yields correct evolutions for the moments. For instance, with a Heaviside initial condition $c_0(x) = H(x)$ and knowing that the PDF f_W of W is a centered Gaussian of variance t $[f_W(W) = (1/\sqrt{2\pi t})e^{-W^2/2t}]$, one obtains, for the scalar mean,

$$\langle c \rangle(x,t) = \int_{-\infty}^{\infty} H(x - \sqrt{2\Gamma}W) f_W dW = \frac{1}{2}\left[1 + \mathrm{erf}\left(\frac{x}{2\sqrt{\Gamma t}}\right)\right]. \tag{48}$$

This expression is also the one obtained directly from the scalar mean equation (43).

B. Pure turbulent advection, bounded domain: Impact of boundary conditions

Let us consider now a bounded domain in order to illustrate the impact of boundary conditions on the solution of Eq. (41). The domain after proper normalization is [0, 1] and the boundary conditions for the PDF f_c are chosen to be $f_c = \delta(c)$ at $x=0$ and $f_c = \delta(c-1)$ at $x=1$. This corresponds for the stochastic field of Eq. (41) to the boundary conditions $c=0$ at $x=0$ and $c=1$ at $x=1$. However, if the simultaneous specification of two boundary conditions is necessary for the diffusion equation of the PDF f_c, it is not the same for the stochastic field $c(x,t)$, due to the advective nature of Eq. (41). For instance, at $x=0$, the $c=0$ inflow condition is only effective when dW is positive and it becomes an outflow condition when dW is negative and reciprocally at $x=1$.

What might seem more surprising is that with any arbitrary initial conditions, the limit when $t \to \infty$ of the solution of Eq. (41) can be shown to be a step whose position is moved randomly by the Brownian motion in interval [0, 1]. Thus, initial profiles, even continuous, are transformed into discontinuous ones due to the influence of boundary conditions. This process can be loosely explained as follows: when dW is positive, part of the initial profile is advected beyond the $x=1$ boundary. When dW becomes negative, this initial information is lost, as it is replaced by the inflow value at $x=1$ boundary. The same also happens at the $x=0$ boundary,

where initial information is replaced by the inflow value at $x=0$. This process is then repeated at both boundaries until eventually, with probability 1, the initial information is lost and only the information given by both boundaries remains.

The evolution described above can be formalized by introducing two supplementary stochastic processes W^+ and W^-:

$$W^+(t) = \max_{s\in[0,t]} (\sqrt{2\Gamma}W(s), W(s) > 0),$$

$$W^-(t) = -\min_{s\in[0,t]} (\sqrt{2\Gamma}W(s), W(s) < 0). \tag{49}$$

Without boundary conditions, W^+ gives the maximum deviation of the initial profile towards positive x and W^- gives the maximum deviation of the initial profile towards negative x. When $W^+<1$, W^+ gives the maximum extent of the initial profile that has crossed the $x=1$ limit. Identically, when $W^-<1$, W^- gives the maximum extent of the initial profile that has crossed the $x=0$ limit.

Now reintroducing boundary conditions, W^+ gives the length of the initial profile modified by the $x=1$ boundary, while W^- gives the one modified by the $x=0$ boundary. This result is valid for times smaller than the time t_S for which the initial condition is converted into a step. This happens when all the initial profile has crossed at least one of the boundaries. t_S is given by

$$t_S = \min_{s\in[0,+\infty]} \{s, W^+(s) + W^-(s) = 1\}. \tag{50}$$

With probability 1, t_S is finite, as, for instance, $\sqrt{2\Gamma}W$ will be greater than 1 with probability 1. Then, for times $t<t_S$, the solution is given by

$$c(x,t) = C_W(x - \sqrt{2\Gamma}W(t)), \tag{51}$$

$$with\ C_W(x) = \begin{cases} c_0(x), & W^- < x < 1 - W^+, \\ 0, & x < W^-, \\ 1, & x > 1 - W^+. \end{cases} \tag{52}$$

Figure 1 illustrates some moments of the conversion between an initial linear profile and a step. This figure was obtained from Eq. (51). A time step $\Delta t=0.08$ was chosen in order to compute the processes W^+ and W^-.

C. Influence of chemical source terms

To illustrate the influence of a source term on the spatial length scale of the scalar field, a source denoted $S(c)$ is added to Eq. (41), solved on an unbounded domain:

$$\frac{\partial c}{\partial t}dt + \sqrt{2\Gamma}\frac{\partial c}{\partial x} \circ dW = S(c)dt. \tag{53}$$

The corresponding equation for the gradient ∇c of the scalar is then given by

$$\frac{\partial \nabla c}{\partial t}dt + \sqrt{2\Gamma}\frac{\partial \nabla c}{\partial x} \circ dW = \frac{\partial S}{\partial c}(c)\nabla c dt. \tag{54}$$

If, for the sake of simplicity, we exclude the possibility for ∇c to be zero, we can rewrite Eq. (54) as

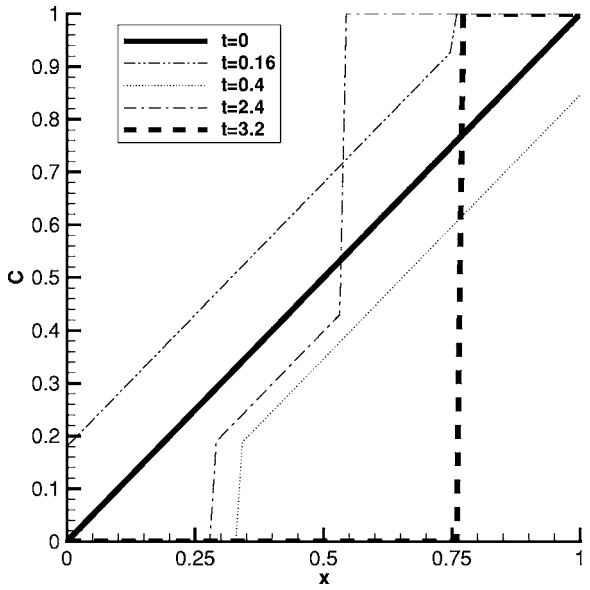

FIG. 1. Formation of discontinuities due to boundary conditions.

$$\frac{\partial}{\partial t}(\ln|\nabla c|)dt + \sqrt{2\Gamma}\frac{\partial}{\partial x}(\ln|\nabla c|) \circ dW = \frac{\partial S}{\partial c}(c)dt. \tag{55}$$

From this equation, it can be seen that a positive gradient in composition space of the source term will enhance the gradient of the scalar field in physical space, while a negative one will have the opposite effect.

It is also observed that a constant turbulent advection velocity does not have any enhancement or attenuating effect on the scalar gradient, but only transports it (this would not be the case if Γ was varying in space). In this regard, the Ito formulation is once again deceptive. Indeed, with Ito interpretation, SPDE (53) can be rewritten as

$$\frac{\partial c}{\partial t}dt + \sqrt{2\Gamma}\frac{\partial c}{\partial x}dW = \Gamma\frac{\partial^2 c}{\partial x^2}dt + S(c)dt. \tag{56}$$

From this formulation, one could have concluded hastily that the second-order differential operator $\Gamma\partial^2 c/\partial x^2$ could balance the influence of the source term. However, as explained in the previous sections, this operator is part of the advection process, along with the stochastic product $\sqrt{2\Gamma}(\partial c/\partial x)\,dW$, and its effects cannot be analyzed independently from this last term.

To illustrate these assertions, let us consider Eq. (53) with the source term $S_a(c)$ given by Eq. (36). From Eqs. (53) and (54), it can be shown that the quantity $\nabla c/S(c)$ is preserved along the characteristic path $dx=\sqrt{2\Gamma}\,dW$. Indeed, along a characteristic path, we have

$$d\left(\frac{\nabla c}{S}\right) = \frac{1}{S}d(\nabla c) - \nabla c\frac{dS}{S^2} = \frac{1}{S}\left[d(\nabla c) - \nabla c\frac{1}{S}\frac{\partial S}{\partial c}dc\right]$$

$$= \frac{1}{S}\left[\frac{\partial S}{\partial c}\nabla c - \nabla c\frac{1}{S}\frac{\partial S}{\partial c}S\right] = 0. \tag{57}$$

Then, while $c<1$, the gradient of the scalar field ∇c is related to the initial gradient ∇c_0 by

$$\nabla c(x,t) = \frac{S_a(c(x,t))}{S_a(c_0(x^*))} \nabla c_0(x^*), \tag{58}$$

where $x^* = x - \sqrt{2\Gamma}W$. This equality is actually valid for any source term which is not zero on the interval [0, 1]. From this relation it is seen that, for $c > c_a$ and $c_0 < c_a$, the gradient of the scalar field is amplified by a factor $1/\varepsilon \gg 1$.

Thus, due to the presence of a stiff chemical source term in Eq. (19), the length scale down to which the stochastic field must be solved can become much smaller than the length scale imposed by the sole velocity field. This picture, however, does not account for the influence of micromixing, which has the potentiality to counteract the effects of stiff source terms.

D. Influence of micromixing on scalar discontinuities

In the example given in Sec. V A 2, it has been shown that spatial discontinuities in the scalar field were likely to appear because of boundary conditions. In this subsection, the effect of micromixing on discontinuities is assessed. To this end, the micromixing term given by the IEM model (10) with a constant mixing frequency ω is added to Eq. (41):

$$\frac{\partial c}{\partial t}dt + \sqrt{2\Gamma}\frac{\partial c}{\partial x} \circ dW = -\omega(c - \langle c \rangle)dt. \tag{59}$$

This equation is solved on an unbounded domain and the initial solution is chosen discontinuous: $c_0(x) = H(x)$, where H is the Heaviside function. The solution to this problem is then given by

$$c(x,t) = H(x - \sqrt{2\Gamma}W(t))e^{-\omega t} + \int_0^t \omega e^{-\omega(t-s)} \langle c \rangle (x - \sqrt{2\Gamma}[W(t) - W(s)], s)ds, \tag{60}$$

where $\langle c \rangle$ is given by Eq. (48).

Thus, this example shows that the micromixing term does not in general suppress discontinuities. However, it will decrease their amplitude and thus minimize their impact. This conclusion is not altered by the presence of a stochastic term in the micromixing model, as in the Langevin model (11).

For instance, let us consider an unbounded scalar and the following micromixing model, mimicking the Langevin model:

$$M = -\omega(c - \bar{c}) + b\dot{W}, \tag{61}$$

where b is a constant. interpretations. If instead of the micromixing term (10), the term (61) is added to Eq. (41), then the evolution of the scalar field is given by

$$c(x,t) = H(x - \sqrt{2\Gamma}W(t))e^{-\omega t} + \int_0^t \omega e^{-\omega(t-s)} \langle c \rangle (x - \sqrt{2\Gamma}[W(t) - W(s)], s)ds + \int_0^t e^{-\omega(t-s)} \circ dW(s), \tag{62}$$

where $\langle c \rangle$ is still given by Eq. (48). Thus, the initial discontinuity is still present and its intensity decreases as time increases.

VI. NUMERICAL ASPECTS

A. Numerical scheme

1. Spatial and temporal discretizations

The numerical analysis focuses on the equation with Stratonovitch interpretation, Eq. (19). Its numerical integration is considered in terms of weak convergence and accuracy. Due to the advection properties of Eq. (19), it might be interesting to use semi-Lagrangian methods to solve it. However, only fully Eulerian schemes will be considered hereafter.

Temporal integration is addressed by recasting Eq. (19) in an SODE form; this allows the use of traditional SODE techniques [13]. An explicit first-order scheme is chosen, with a predictor-corrector procedure generalizing the Heun scheme [16].

As for spatial discretization, scalar fluxes are interpolated with a second-order essentially nonoscillatory (ENO) scheme and a decentered procedure is used for the advection term. Decentering derivatives yields a correlation between the white noise and the discretization error [17]. As a result, despite the second-order interpolations, the resulting scheme is only first order in space.

2. Boundary conditions

The issue of boundary conditions is also a crucial one and will be dealt with more thoroughfully in future work. In this article, boundary conditions with first-order accuracy are applied. It should be noted that a diffusion equation like the one for the PDF requires boundary conditions to be specified on all the domain frontiers, whereas a hyperbolic equation only requires boundary conditions to be specified on certain parts of the frontier.

Furthermore, the turbulent stochastic advection term of Eq. (19) can change the specification of boundary conditions in time. For instance, for the simplified case considered in Sec. V, the boundaries alternatively become inflow boundaries, with a specified value of the stochastic field or outflow boundaries, with a value of the stochastic field computed from the interior of the domain.

B. Numerical tests

1. Description

The purpose of the numerical calculations described hereafter is to assess the tractability of the EMC method introduced in the previous sections and also to check the statistical and spatial convergence of the numerical scheme proposed in Sec. VI A. To this end, we consider a simplified one-dimensional version of the scalar PDF equation (9), with constant density ρ=const and constant mean velocity $\tilde{U}$

$=U_0$. The calculation is performed on a domain of length L. As in [18], we define dimensionless quantities, based on the domain length and on a reference velocity U:

$$t^* = tU/L, \quad x^* = x/L, \quad U_0^* = U_0/U,$$

$$\mathcal{M}^* = \mathcal{M}L/U, \quad \omega^* = \langle \omega_c \rangle L/U,$$

$$\Gamma^* = \Gamma_T/(UL), \quad S = S^* L/U. \tag{64}$$

In the remainder of this section, only dimensionless quantities will be considered. For the sake of clarity, the notation with exponent $*$ will be dropped. is considered.

The dimensionless PDF equation is then given by

$$\frac{\partial f_c}{\partial t} + U_0 \frac{\partial f_c}{\partial x} = \frac{\partial}{\partial x}\left(\Gamma \frac{\partial f_c}{\partial x}\right) - \frac{\partial}{\partial s}(\mathcal{M} f_c + S f_c). \tag{65}$$

The computational domain (after normalization) [0, 1] and the boundary conditions are at $x=0$, $f_c=\delta(c)$ and at $x=1$, $f_c=\delta(c-1)$. The initial condition is chosen to be $f_c=\delta(c-1)$.

The simplified version of Eq. (19) corresponding to the PDF equation (65) is

$$\frac{\partial c}{\partial t} + \left(U_0 - \frac{1}{2}\frac{\partial \Gamma}{\partial x}\right)\frac{\partial c}{\partial x} + \sqrt{2\Gamma}\dot{W} \circ \frac{\partial c}{\partial x} = M + S. \tag{66}$$

The corresponding boundary conditions are $c(t,x=0)=0$, when $\dot{W}>0$ and $c(t,x=1)=1$ when $\dot{W}<0$. The specification of both boundaries at the same time is not possible due to the hyperbolic nature of Eq. (66). The initial condition corresponding to the initial PDF is $c_0(t=0,x)=1$.

Four tests are performed. In the first one, the impact of the discontinuities described in Sec. V is assessed. In this first case, Eq. (66) is solved with constant turbulent diffusion, no micromixing, and no chemical source term: $M=0$, $S=0$, $U_0=0$, and $\Gamma=\Gamma_0$, where Γ_0 is a constant. To study statistical convergence, a velocity $U_0=0$ is chosen, while spatial convergence is examined with mean velocity $U_0=1$. The addition of a mean velocity sharpens the moment profiles and requires a greater spatial accuracy from the numerical scheme.

In the second test, the influence of micromixing on the spatial and statistical convergences is evaluated. Compared to the first test, the IEM micromixing model defined by Eq. (10) is added. In this test, a constant mixing frequency is chosen: $\omega=$const.

In the third test, Γ is chosen to be variable and the role of the drift velocity [Eq. (18)] is analyzed. Compared to the second test, the coefficient Γ is changed to

$$\Gamma = \Gamma_0[1 - 14x^2(1-x)^2]. \tag{67}$$

In the last test, the properties of the EMC method in presence of a nonlinear source term are examined. The following nonlinear Arrhenius source term, typical of exothermic reactions taking place in combustion processes, is considered:

$$S = 21830c(1-c)e^{-20/(1+3c)}. \tag{68}$$

Besides, two micromixing models are examined, the IEM model [Eq. (10)] and the Langevin model [Eq. (11)]. For both models, the mixing frequency is chosen constant: $\omega=$const.

Some of the cases described above correspond to the ones examined in [3] and [18]. In agreement with those studies, the nondimensionnalized [18] values $\Gamma_0=0.1$ and $\omega=20$ are chosen. When it is not zero, the value of U_0 is chosen equal to 1. In the Langevin model, the value of the constant d_0 is set to 1.

2. Numerical procedure

The numerical scheme described in Sec. VI A yields the following discretization for SPDE (66):

$$c_i^{n+1} = c_i^n - (U_0\Delta t + \sqrt{2\Gamma\Delta t}\xi^n)\frac{c_{i+1/2}^{n+1/2} - c_{i-1/2}^{n+1/2}}{dx} + M(c_i^{n+1/2})\Delta t + S(c_i^{n+1/2})\Delta t, \tag{69}$$

where

$$c^{n+1/2} = \frac{1}{2}(c^* + c^n), \tag{70}$$

$$c_i^* = c_i^n - (U_0\Delta t + \sqrt{2\Gamma\Delta t}\xi^n)\frac{c_{i+1/2}^n - c_{i-1/2}^n}{dx} + M(c_i^n)\Delta t + S(c_i^n)\Delta t. \tag{71}$$

The i indexes correspond to a regular mesh with N_c cells of size Δx. The n exponents correspond to the successive instants $t_0+n\Delta t$, with Δt constant. The values of c at cell interfaces $c_{i\pm1/2}$ are interpolated with an ENO procedure and decentered. A cfl condition is enforced:

$$\Delta t = \mathrm{cfl}\frac{\Delta x^2}{U_0\Delta x + 2\Gamma}, \tag{72}$$

where $\mathrm{cfl}<0.5$ due to the presence of the ENO interpolant. ξ_n is a stochastic noise. It is shown in [17] that a binomial noise (equal to ±1 with equal probability) is sufficient to ensure the precision of the numerical scheme as given in Sec. VI A.

Equation (69) is solved for N stochastic fields $\{c^{(k)}, k=1,\ldots,N\}$ and with N independent noises $\xi^{(k)}$. The mean of a function $Q(c)$ is simply computed by

$$\langle Q(c)\rangle_i^n = \frac{1}{N}\sum_{k=1}^{N} Q(c_i^{n,(k)}). \tag{73}$$

A convergence error is defined for stationary problems and for each moment of c:

$$e_p = \sum_{i=1}^{N_c} \left|\langle c^p\rangle_i - \langle c^p\rangle_{ref}(x_i)\right|, \tag{74}$$

where $\langle c^p\rangle_{ref}(x_i)$ is a reference solution of the problem at point x_i. When the right-hand side of SPDE (66) is null (test 1), an analytic solution exists and is used as the reference solution. When the right-hand side of SPDE (66) is linear

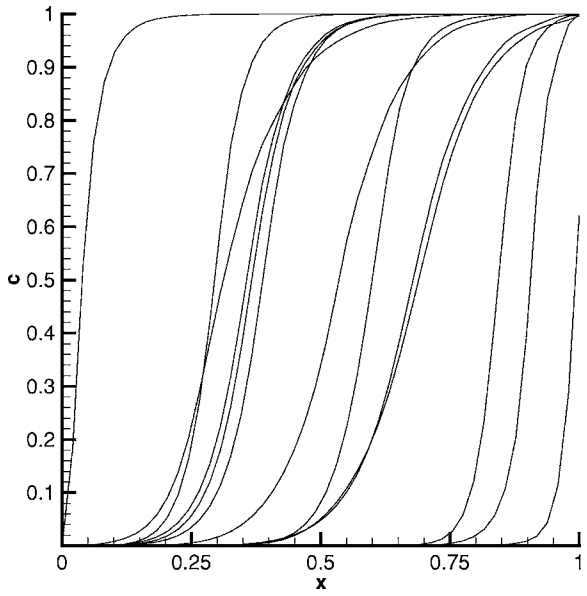

FIG. 2. Test 1: no micromixing $\omega=0$, no source term $S=0$, $\Gamma=0.1$, $U_0=0$. Stochastic fields at time $t=10$.

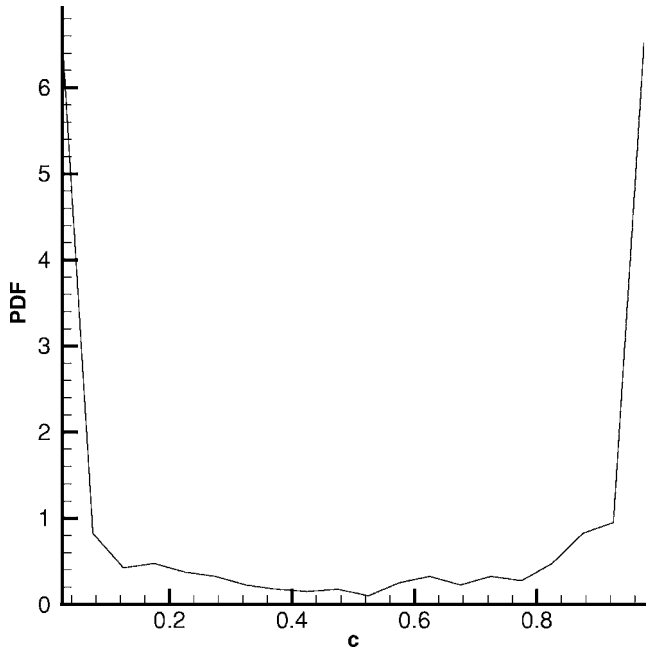

FIG. 3. Test 1: no micromixing $\omega=0$, no source term $S=0$, $\Gamma=0.1$, $U_0=0$. PDF at $t=10$ and $x=0.51$.

(tests 2 and 3), an analytic solution also exists, but its expression is not directly used. It is sufficient and more practical for our purpose to solve the equations for the moments with a finite-difference method. For the fourth test, the source term is nonlinear, and no analytic solution can be obtained. Instead, we use a finite-difference method to solve the equation for the distribution function—i.e., the integral of the PDF (65) with respect to c.

When not mentioned, the default values of N_c and N in the following calculations are $N_c=50$ and $N=100$.

3. *Influence of discontinuities on statistical and spatial convergence*

In Sec. V, it has been shown that discontinuities can be created by the hyperbolic nature of the equations and the influence of boundary conditions. In this first numerical test, the impact of such discontinuities on the numerical statistical and spatial convergence is assessed.

First, Eq. (66) is solved without a micromixing or chemical source term, with $\Gamma=\Gamma_0$ and with $U_0=0$. As shown in Sec. V B, the solution of Eq. (66) then consists in a step which position is random. This implies that, in theory, only two values of the scalar field can be obtained: 0 and 1. In other words, the PDF is made of two Dirac peaks located at $c=0$ and $c=1$. The stationary solution of the PDF equation is given by

$$f_c(c;x) = (1-\langle c\rangle)\,\delta(c) + \langle c\rangle\,\delta(c-1),$$

$$\langle c\rangle = x. \tag{75}$$

From Eqs. (75), it follows that

$$\langle c^p\rangle = x, \quad p = 1,2,3,\ldots\ . \tag{76}$$

Figure 2 shows several stochastic realizations computed from Eq. (66) after statistical convergence is reached (the default values of N_c and N_p are taken).

Due to numerical diffusion, the computed profiles are not strictly steps, but present a continuous, even if sharp, variation between 0 and 1. As a consequence, new potential values are introduced by numerical diffusion, so that the PDF is not made any longer of two Dirac peaks. Instead (see Fig. 3), it presents two peaks at $c=0$ and $c=1$, as well as a ground value between 0 and 1. This additional component in the PDF introduces a bias in the computation of the moments of order greater than 1 and induces strong limitations on their convergence. Figure 4 shows the statistical convergence of moments of order $p=1,\ldots,6$. Due to symmetry reasons, convergence of the mean is not affected and follows the $N^{-1/2}$ theoretical law. However, convergence of higher-order moments is slowed down and rapidly stagnates. Figure 5 illustrates the effects of numerical diffusion on the computed moments. It is seen that higher-order moments do not correspond to the analytic solution.

To study spatial convergence, a velocity $U_0=1$ is added. It is observed in Fig. 6 that discontinuities also have a negative effect on spatial convergence. The first-order precision of the numerical scheme is lost. For the first and second moments, the scheme appears as a 0.6 order, while for other moments, there is no convergence at all.

Thus, this first test case exhibits the need to use numerical methods capable of handling advection of discontinuous scalar fields with as small a numerical diffusion as possible. Indeed, the smearing of discontinuities yields a bias proportional to the length on which the discontinuities are spread. It must be stressed that the particular case under scrutiny is unfavorable to EMC methods: the solution is only made of discontinuities and puts forward any difficulty in computing them. Such a case is actually not encountered in practical calculations, in which one must at least account for the additional effects of micromixing.

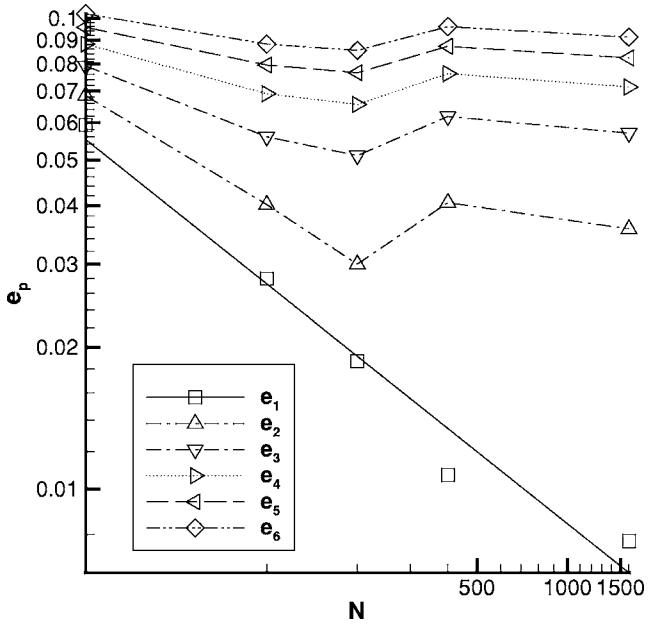

FIG. 4. Test 1: no micromixing $\omega=0$, no source term $S=0$, $\Gamma=0.1$, $U_0=0$. Statistical convergence of the moments: error e_p against the number of stochastic fields, N.

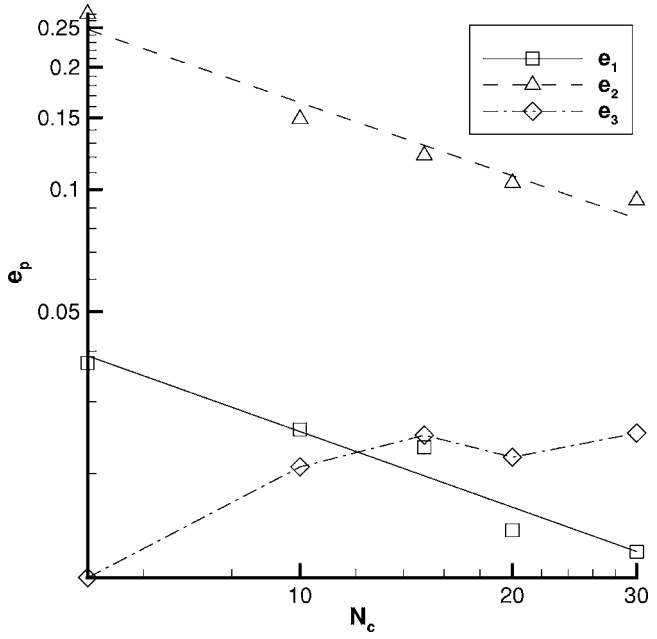

FIG. 6. Test 1: no micromixing $\omega=0$, no source term $S=0$, $\Gamma=0.1$, $U_0=1$. Spatial convergence: error e_p against the number of cells, N_c.

4. Influence of micromixing on scalar discontinuities

In the second test case, the IEM micromixing model is added to Eq. (66), with $\omega=20$, while all parameters are kept constant compared to the first test. A reference solution is obtained for this problem by solving the moment equations with a finite difference (FD) method. The equation for the moment of order p is

$$\frac{\partial\langle c^p\rangle}{\partial t}+U_0\frac{\partial\langle c^p\rangle}{\partial x}=\frac{\partial}{\partial x}\left(\Gamma\frac{\partial\langle c^p\rangle}{\partial x}\right)-p\omega[\langle c^p\rangle-\langle c\rangle\langle c^{p-1}\rangle]. \tag{77}$$

For solving this equation, one needs to know the moment of order $p-1$. As a consequence, to compute $\langle c^p\rangle$, one has to solve all moments of order $n<p$.

We first take $U_0=0$ and examine how scalar-field discontinuities are affected by micromixing. It can be seen in Fig. 7 that stochastic scalar profiles still present discontinuities nearby the boundaries $x=0$ and $x=1$. It can be seen in Fig. 7 that these discontinuities are still numerically diffused. However, micromixing diminishes their amplitude and restrains their influence close to boundaries. Besides, with the addition of micromixing, the solution does not depend only on an accurate prediction of discontinuous profiles, but also on the smooth evolution of the profiles on each side of the discontinuity. As a result, statistical convergence is found to follow the theoretical $N^{-1/2}$ law, as seen in Fig. 8, and a good agreement is found between analytical and computed mean profiles (Fig. 9).

Similarly, spatial convergence is also recovered (see Fig. 10). As in the previous section, this figure was obtained for $U_0=1$.

Thus, this second example shows that, thanks to the additional effects of micromixing, discontinuities might not be as impairing as suggested by the first example. This, however, does not alleviate the fact that discontinuities must be treated correctly.

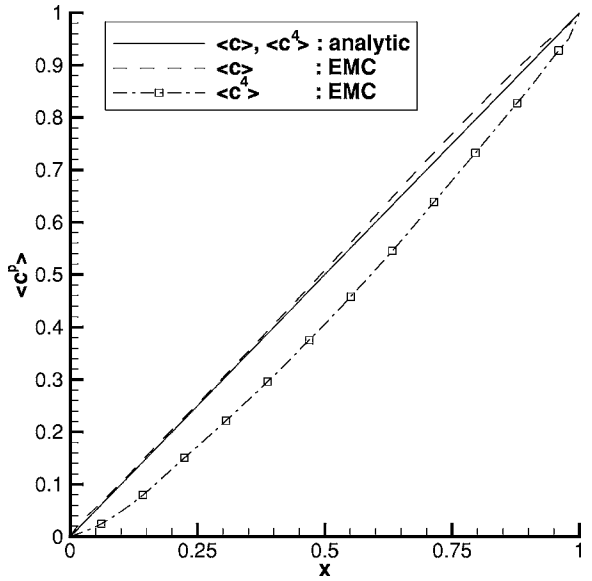

FIG. 5. Test 1: no micromixing $\omega=0$, no source term $S=0$, $\Gamma=0.1$, $U_0=0$. Comparison of the moments computed with the EMC method against the analytic solution [Eq. (76)].

5. Influence of the spatial variations of the stochastic velocity

In case the stochastic velocity varies with space, it has been shown in Sec. III that a deterministic drift velocity [Eq.

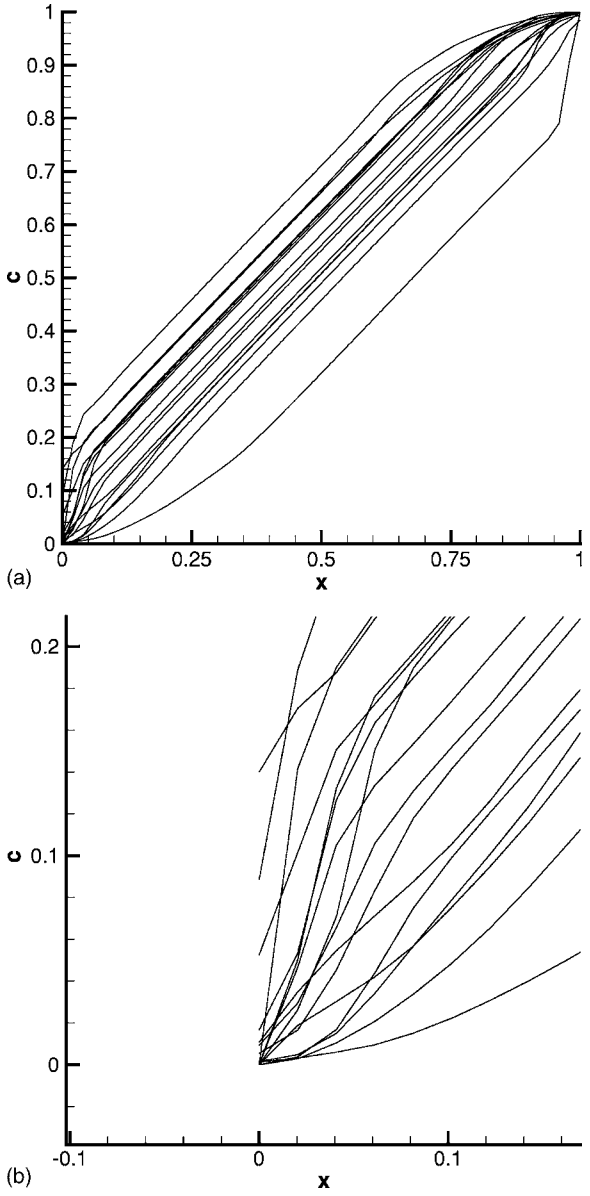

FIG. 7. Test 2: IEM model $\omega=20$, no source term $S=0$, $\Gamma=0.1$, $U_0=0$. (a) Stochastic fields at time $t=10$; (b) zoom-in the stochastic fields in the vicinity of $x=0$.

(18)] had to be added. To analyze the influence of this drift velocity on convergence, Eq. (41) is solved with Γ defined by Eq. (67), with $U_0=0$ and all other parameters kept constant in respect with the second test.

With this setting, it is observed (see Fig. 11) that the $N^{-1/2}$ convergence rate is actually respected, which confirms the derivation of the correction velocity. Figure 12 illustrates some of the moments obtained with a variable diffusion coefficient.

6. Influence of nonlinear source terms

For this problem, a reference solution is obtained by solving, with a finite-difference method, the distribution function

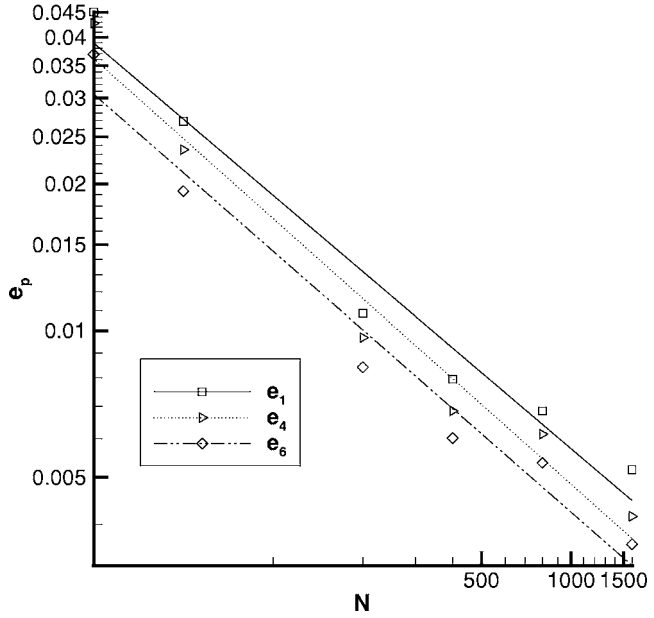

FIG. 8. Test 2: IEM model $\omega=20$, no source term $S=0$, $\Gamma=0.1$, $U_0=0$. Statistical convergence: error e_p against the number of stochastic fields, N.

$$F_c(c) = \int_0^c f_c(\psi)d\psi. \tag{78}$$

The reason for working with F_c, rather than the PDF f_c comes from the definition of boundary conditions at $c=0$ and $c=1$. For the PDF, these are given by two Dirac peaks, while for the distribution function, they are, respectively, given by $F_c(0)=0$ and $F_c(1)=1$. Boundary conditions for F_c are easier

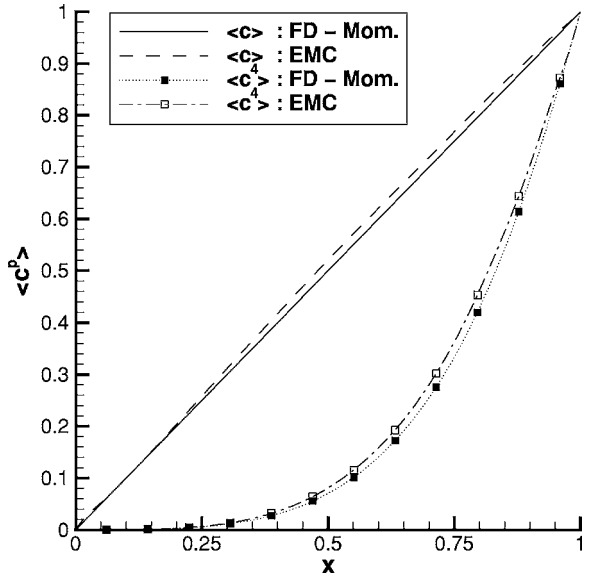

FIG. 9. Test 2: IEM model $\omega=20$, no source term $S=0$, $\Gamma=0.1$, $U_0=0$. Comparison of the moments computed with the EMC method against the reference solution (FD-Mom.). The reference solution is computed from the moment equation (77) with a finite difference (FD) method.

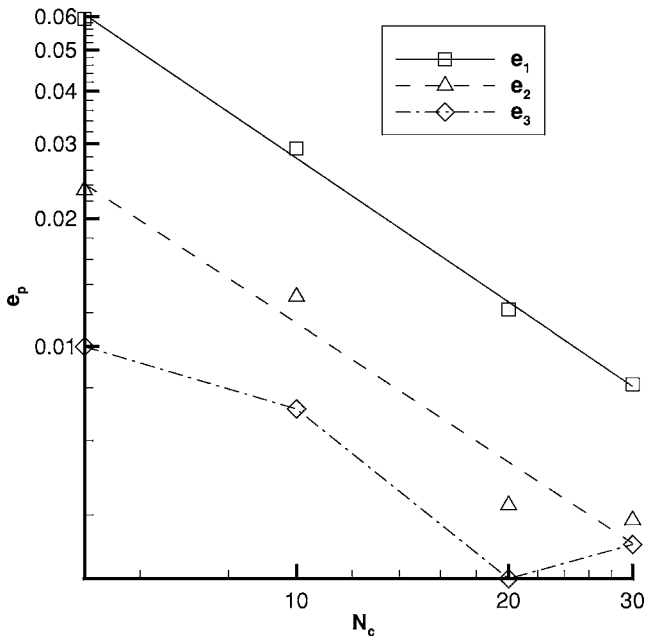

FIG. 10. Test 2: IEM model $\omega=20$, no source term $S=0$, $\Gamma=0.1$, $U_0=1$. Spatial convergence: error e_p against the number of cells, N_c.

to handle from a numerical point of view and allow one to improve the accuracy of the calculation. The equation for F_c is directly deduced from Eq. (65) by integrating it with respect to c:

$$\frac{\partial F_c}{\partial t} + U_0 \frac{\partial F_c}{\partial x} = \frac{\partial}{\partial x}\left(\Gamma \frac{\partial F_c}{\partial x}\right) - \left(\mathcal{M}\frac{\partial F_c}{\partial c} + S\frac{\partial F_c}{\partial c}\right). \quad (79)$$

Moments are then directly commputed by the formula

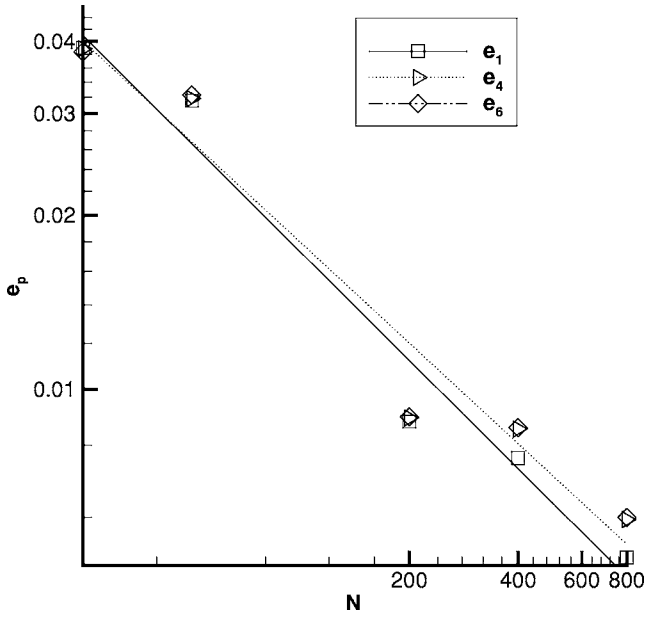

FIG. 11. Test 3: IEM model $\omega=20$, no source term $S=0$, $\Gamma=0.1[1-14x^2(1-x)^2]$, $U_0=0$. Statistical convergence: error e_p against the number of stochastic fields, N.

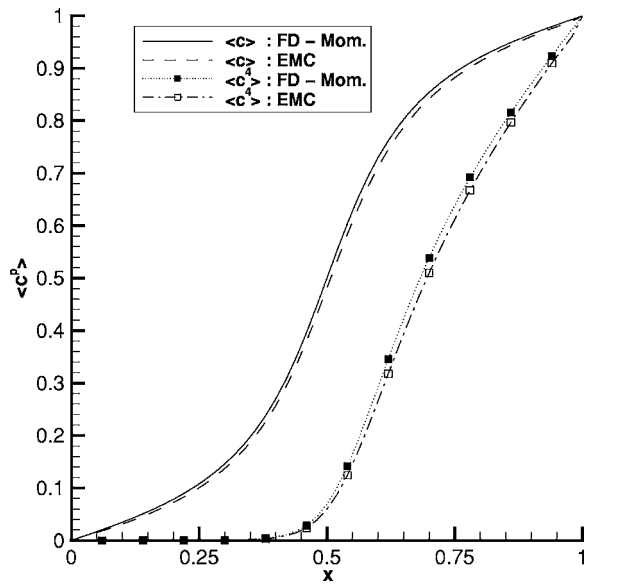

FIG. 12. Test 3: IEM model $\omega=20$, no source term $S=0$, $\Gamma=0.1[1-14x^2(1-x)^2]$, $U_0=0$. Comparison of the moments computed with the EMC method against the reference solution (FD-Mom.). The reference solution is computed from the moment equation (77) with a finite-difference (FD) method.

$$\langle c^p \rangle = 1 - p\int_0^1 c^{p-1} F_c dc. \quad (80)$$

A first calculation is performed with the stiff nonlinear source term defined by Eq. (68) and with the IEM micromixing model. The profiles are shown in Fig. 13. As argued in Sec. V, strong gradients are indeed observed. The mean values obtained by solving the PDF equation with a finite-difference method and with the EMC method are shown in Fig. 14. It is seen that the two methods yield different results. For the EMC method, it is likely that the numerical diffusion

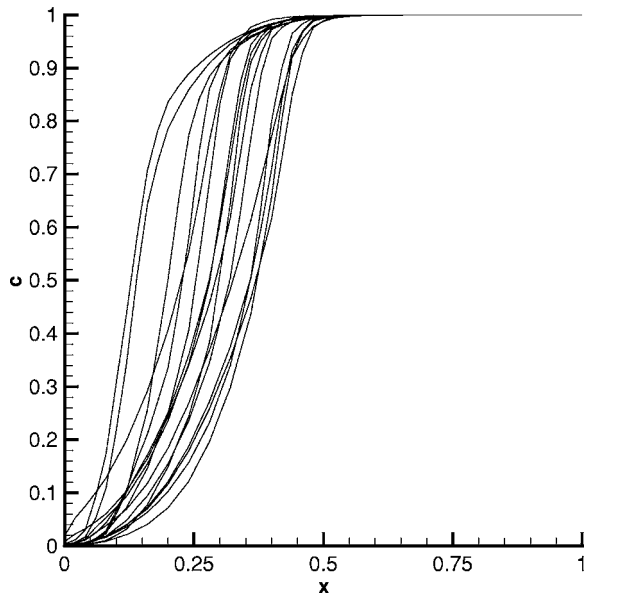

FIG. 13. Test 4: IEM model $\omega=20$, Arrhenius nonlinear source term, $\Gamma=0.1$, $U_0=1$. Stochastic fields at time $t=10$.

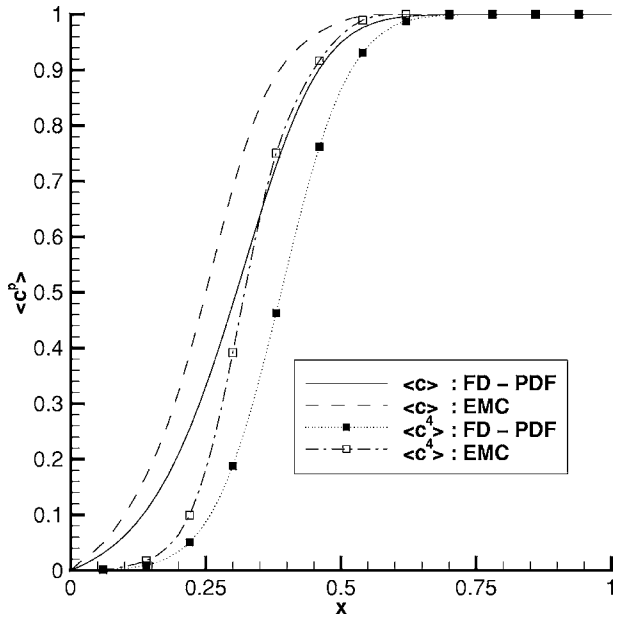

FIG. 14. Test 4: IEM model $\omega=20$, Arrhenius nonlinear source term, $\Gamma=0.1$, $U_0=1$. Comparison of the moments computed with the EMC method against the reference solution (FD-PDF). The reference solution is computed from Eq. (79) with a finite-difference (FD) method.

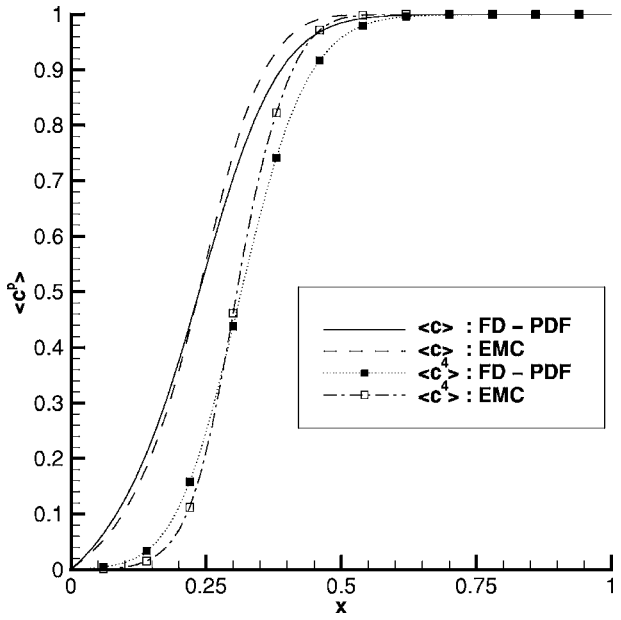

FIG. 15. Test 4: Langevin model $\omega=20$, $d_0=1$, Arrhenius nonlinear source term, $\Gamma=0.1$, $U_0=1$. Comparison of the moments computed with the EMC method against the reference solution (FD-PDF). The reference solution is computed from Eq. (79) with a finite-difference (FD) method.

of the gradients biases the solution. As for the finite-difference solution of the PDF equation, it might altered by the presence of Dirac peaks at boundaries. One of the difficulties in solving the PDF equation (65) with a stiff source term along with the IEM model is that the evolution of the PDF in composition space is hyperbolic and also subject to rapid variations that will enhance discrepancies along characteristic paths in composition space. One can then expect that the addition of a diffusion term in composition space will attenuate this effect.

Indeed, if one uses the Langevin model instead of the IEM model, then one obtains a good agreement between the two methods. Thus, Fig. 15 shows some moments computed with the Langevin model by both methods and Fig. 16 shows that EMC method solution converges towards the solution obtained with the finite-difference method.

7. Comparison with LMC methods

To allow comparison against traditional LMC methods, SODE's (33) with simplifications corresponding to Eq. (34) are solved. The number of particles per cell is denoted N_{pc}. Particle means are computed by a simple first-order interpolation formula

$$\langle Q\rangle_i = \frac{1}{N_{pc\,particle}} \sum_{(k)\in cell\ i} Q(c^{(k)}). \tag{81}$$

A comparison is done in terms of computational effort and precision. Precision is measured by the errors e_p, while computational effort is measured by the CPU time spent to achieve convergence on a single 1.6-GHz processor.

A first comparison is made for the case $U_0=0$, $\Gamma=\Gamma_0$ and with the IEM micromixing model. For this case, it is seen (Fig. 17) that the computational effort required by the EMC method to attain a given accuracy is greater than the one required by the LMC method by at least an order of magnitude.

At the other extreme, if one now compares both methods when $U_0=1$ and $\Gamma=\Gamma_0$ and with the IEM micromixing model, then this tendency is inverted. It is seen (Fig. 18 that both methods give similar results for the computation of the

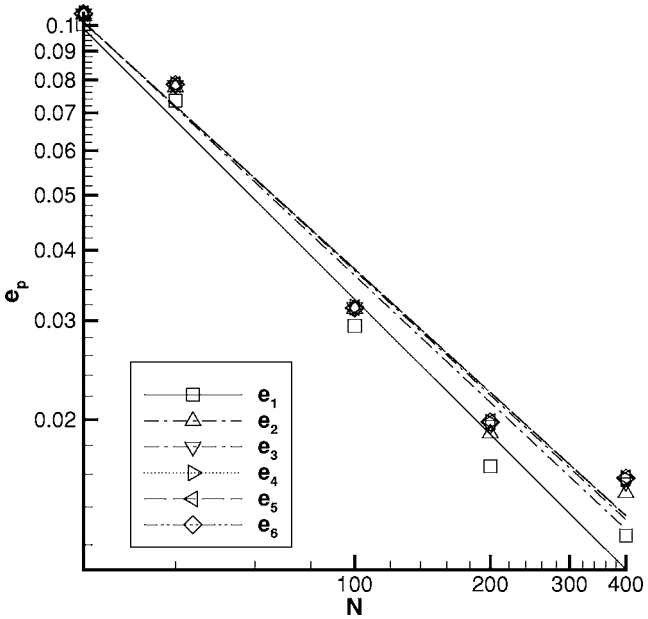

FIG. 16. Test 4: Langevin model $\omega=20$, $d_0=1$, Arrhenius nonlinear source term, $\Gamma=0.1$, $U_0=1$. Statistical convergence: error e_p against the number of stochastic fields, N.

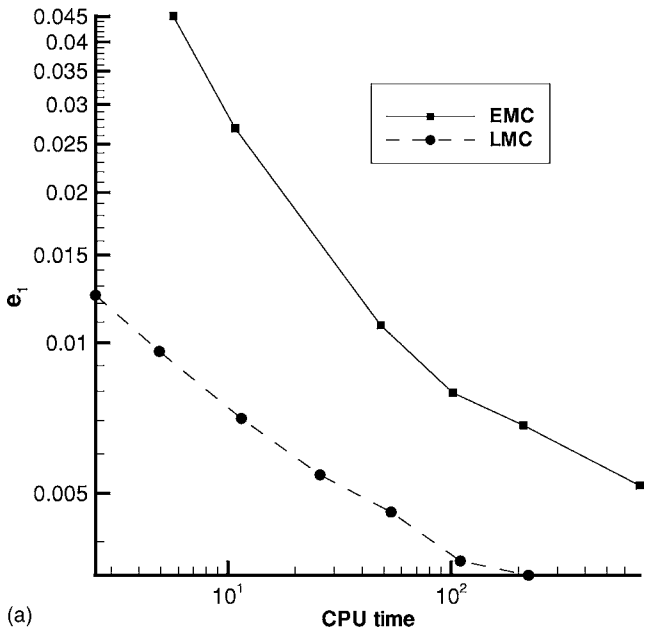

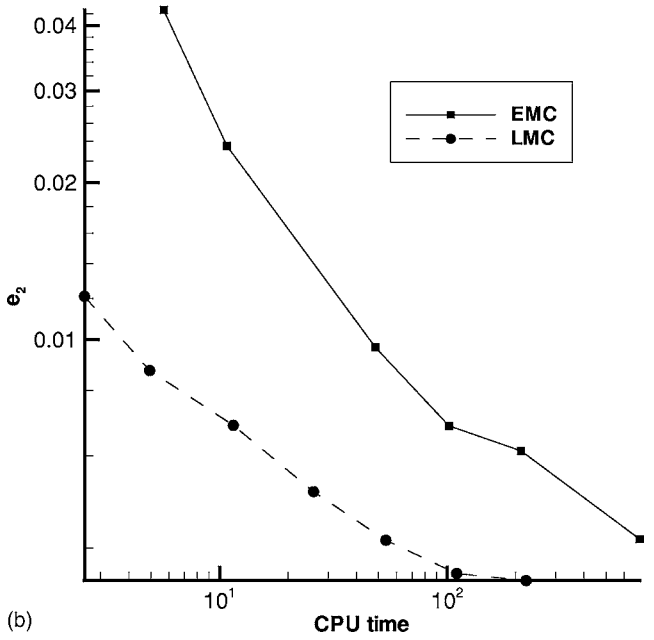

FIG. 17. Comparison EMC/LMC-IEM model $\omega=20$, no source term $S=0$, $\Gamma=0.1$, $U_0=0$. (a) Error e_1; (b) error e_4.

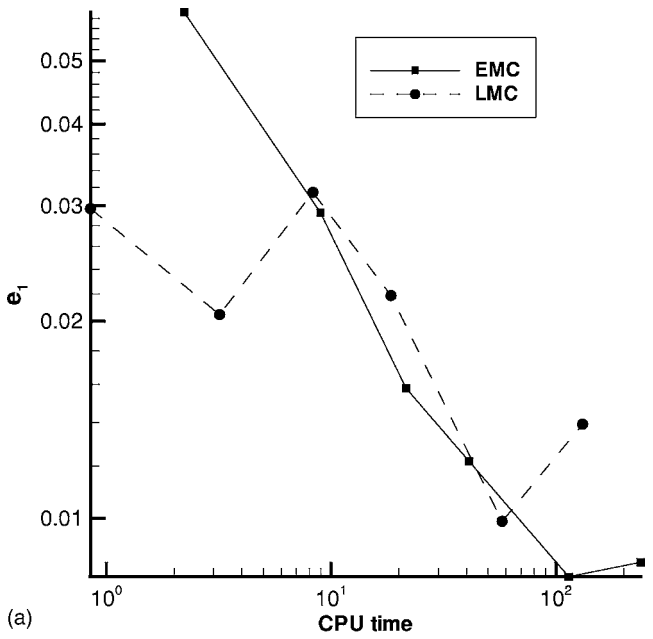

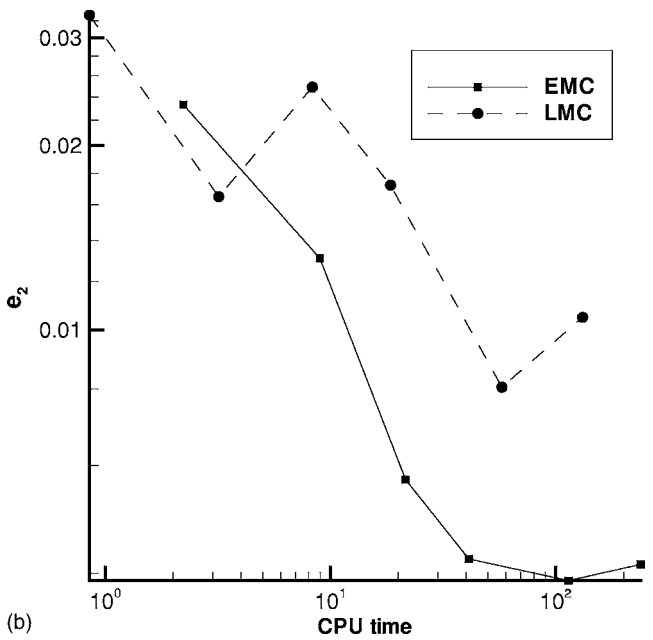

FIG. 18. Comparison EMC/LMC-IEM model $\omega=20$, no source term $S=0$, $\Gamma=0.1$, $U_0=1$. (a) Error e_1; (b) error e_2.

mean, while the EMC method appears as at least an order of magnitude faster for computing higher-order moments. The main difference between these two extremes is that the second case is more demanding in terms of spatial accuracy, as the mean profiles possess stiffer gradients. This tends to indicate that the LMC method is more accurate in terms of statistical precision (as it is not as biased by numerical diffusion), while it is less accurate than the EMC method in terms of spatial precision.

More interestingly, for the more realistic case $U_0=1$, $\Gamma=\Gamma_0$, with the Langevin micromixing model and with the nonlinear source term, it is observed that both methods attain a given precision for an equivalent CPU time (Fig. 19).

VII. DISCUSSION

So far, a new path allowing to derive SPDE's for computing PDF equations has been proposed and illustrated on several analytical and numerical examples. Another more restrictive path for deriving such SPDE's was first proposed by Valiño [3]. In addition, techniques other than EMC methods are also currently used for computing PDF equations. Among them, we can cite the LMC methods but also the finite-volume/difference/element methods and some variants of mesh-free Galerkin and finite-point-set methods. In this section, we would like to address the question of the relative merits and drawbacks of these different methods.

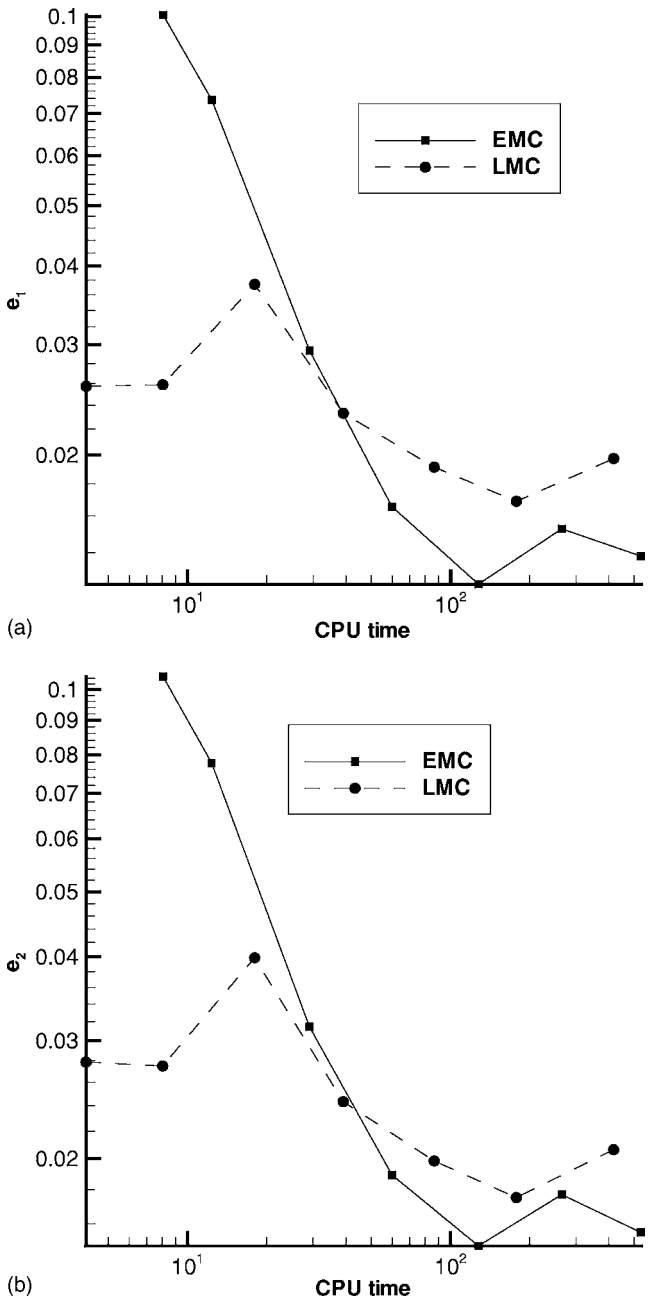

FIG. 19. Comparison EMC/LMC-Langevin model $\omega=20$, $d_0=1$, Arrhenius nonlinear source term, $\Gamma=0.1$, $U_0=1$. (a) Error e_1; (b) error e_2.

A. Field Monte Carlo formulation

EMC methods have been extensively used in several domains (for instance, see [19] for shallow water applications, [20] for quantum mechanics, or [21] for applications of polynomial chaos expansions). However, their application to simulations of turbulent reactive flows only seems to be dating back from Valiño's recent work [3], in which the method is named the field Monte Carlo formulation.

In [3], a connection is established between the PDF equation (9) with the IEM model and the parabolic SPDE's (20) with Ito interpretation. However, the path followed to obtain this connection suffers from several limitations.

First, restrictive hypotheses are used. The connection between the PDF equation and the SPDE's is explicitly limited to smooth, twice differentiable in space stochastic fields. An argument is given suggesting that this restriction is not impairing and that discontinuities can be regarded as pathological: a mapping is introduced to show that the stochastic fields and the PDF have "similar grade of spatial smoothness." However, this last argument only holds if the mapped fields are themselves smooth, which remains an hypothesis. As a matter of fact, it has been shown in Sec. V that discontinuities are on the contrary likely to appear due to the presence of boundary conditions.

Another drawback of the path followed in [3] is that it does not allow one to gain any insight into the obtained equation: Equation (20) is erroneously interpreted in [3] as an advection-diffusion-reaction equation. As shown in Sec. III, it is in fact an advection-reaction equation. This consideration is crucial for building numerical scheme. In this regard, knowledge of the actual advection velocity, only apparent in the Stratonovitch formulation (19), is also crucial.

Thus, despite yielding correct equations (with Ito interpretation), the path followed by Valiño appears as constrained by unnecessary hypothesis and without discussion of physical meaning.

B. About Lagrangian and Eulerian Monte Carlo methods

For the past 20 years, the LMC approach, under its finite-point-set formulation proposed by Pope [2], has been the most popular method for solving PDF equations in the field of turbulent combustion. Its efficiency and accuracy have been proved on many different configurations [12], from academic to industrial ones.

Compared to the EMC method proposed in this article, LMC methods possess one main advantage: in a Lagrangian framework, the information carried by particles is purely local in physical space (if one excepts the computation of means; see paragraph below). There is no gradient to compute and consequently no numerical error due to its discrete approximation. As a result, discontinuities such as the ones described in Sec. V do not exist. Similarly, stiff chemical source terms, even if requiring careful numerical treatment, do not impose length scale restrictions such as those encountered with EMC methods. As already detailed in Secs. V and VI, these two points are the main limits of EMC methods and cannot *a priori* be suppressed except by the use of sophisticated and probably expensive numerical techniques.

On the other hand, a few difficulties may be experienced when using LMC methods. A first difficulty may arise from the sampling error and its impact on the signification of the computed means. For instance, let us consider a constant density flow and let us examine what are the properties of the mean density that would be computed with an LMC method. In LMC methods, the mean density is computed by summing the weights carried by the stochastic particles present in a given cell of the computational domain, and by dividing this sum by the cell volume. If the weights are uniform for all particles, the computed mean density is proportional to the number of particles present in a given cell. But because of

the sampling error, the number of particles will vary in time and also from one cell to another. In other words, the value of the computed mean density will vary both in time and in space. As a consequence, the physical property of constant density will not be respected. Thus, this example points out that, because of the sampling error, computed means in LMC methods might lose some of their physical meaning.

Another point is that the sampling error may not always be controlled with precision. Indeed, it depends on the distribution of stochastic particles in the physical domain, and this distribution is in general not uniform: without correction, the probability of finding a particle at a given location is proportional to the mean density $\langle \rho \rangle$. As a result, the physical domain will possess zones with a high number of particles and a high accuracy as well as zones with a small number of particles and a low accuracy.

To avoid those first two difficulties, one may introduce correction algorithms [22], but the influence of these algorithms on the precision of the calculation, their influence on convergence, and the possibility of applying them in a general case are not yet completely assessed.

Another drawback of LMC methods stems from the extraction of mean quantities from a set of particles. Whatever the method chosen, computing a mean value at a given point involves making weighted sums on particles located in a small spatial surrounding of this point. Thus, the purely local property of the Lagrangian method described in the paragraph above is in practice lost due the numerical evaluation of means. A first consequence is that the computation of means is ambiguous as it does not simply yield an *ensemble average* but also a *spatial filtering* of the computed mean. For RANS calculations, this is obviously not impairing, but when LMC methods are used in conjunction with a LES solver [23], this becomes problematic. In addition, if mean values are introduced in the definition of the velocity of the particles or in the source of the stochastic scalar, then numerical diffusion will also be introduced alongside particle trajectories in composition and physical space. Furthermore, at boundary conditions, δ functions cannot be treated in an exact manner anymore.

Another difficulty may come from the fact that all particles must *a priori* evolve in physical space with the same definition of velocity. On the other hand, accounting for effects such as near-wall molecular diffusion for species with different Schmidt numbers may require different velocities to be prescribed [24].

A last drawback of LMC method is that to improve convergence rates, it is often necessary to couple the LMC method to a Eulerian RANS solver; this can quickly result in a heavy tool to manipulate, due to the different nature (Lagrangian-Eulerian) of the solvers. In addition, this coupling introduces duplicate quantities [22] and requires a correction algorithm to eliminate redundancies. Besides, due to the nonhomogeneous repartition of particles in the spatial domain, particle means may present a noisy aspect, which, if not smoothed, is harmful to the RANS solver.

Finally, both LMC and EMC methods share a common default: the phenomenon of nonuniform particle distribution described for LMC methods in physical space also exists in composition space for both LMC and EMC methods. There are domains in composition space where statistical accuracy is poor due to a lack of stochastic realizations. These domains obviously correspond to rare possible values of the scalar field which might precisely be the ones of interest for some practical applications (see the Introduction). For instance, if the PDF of a scalar c at a given point in space is made of two Dirac peaks at $c=0$ and $c=1$ which combined amplitude is 0.9, then with 100 particles or stochastic fields, one will schematically only have 10 realizations to describe the remaining of the PDF between 0 and 1. In the same way, PDF's with long tails are difficult to represent accurately with LMC and EMC methods. This last defect is the price to pay for exchanging the fixed discretization of composition space offered by full Eulerian methods for the moving one of Monte Carlo methods.

C. About full Eulerian methods, particle and mesh-free methods

It is often argued that, for solving PDF equations, while finite methods yield an exponential growth of the computational cost with the number of dimensions, Monte Carlo methods only yield a linear growth. This last consideration, however, is, in theory, only true for a fixed number of stochastic particles or stochastic fields. If one rather focuses on the the computational effort for a given accuracy, then one can also obtain an exponential increase for Monte Carlo method. To fix ideas, let us consider a LMC calculation on a one-dimensional domain $[0, 1]$ and on a two-dimensional domain $[0,1]\times[0,1]$, both with spatial accuracy $\Delta x=1/N_c$. There are consequently N_c cells in the one-dimensional domain and N_c^2 cells in the two-dimensional one. If we imagine that the desired statistical accuracy is reached for a number of particles per cell, N_{pc}, then we see that a total number of $N_p=N_cN_{pc}$ particles is required for the one-dimensional problem while a number $N_p=N_c^2N_{pc}$ is required for the two-dimensional problem. In d dimensions, $N_p=N_c^dN_{pc}$ particles would have been required.

In fact, the interest of Monte Carlo methods compared to finite methods is that they offer a convenient, versatile way of discretizing the physical and/or composition space. Thus, in practical calculations of turbulent reactive flows, a great number of compositions are considered, but the complete joint PDF is not used as such. Instead, only marginal PDF's of a few (2–3) compositions are involved. In that case, increasing the number of compositions does not increase the number of dimensions of the marginal PDF's which are practically solved. As a result, for practical problems in turbulent reactive flows, a linear growth of the CPU effort is actually obtained with Monte Carlo methods.

This would also be the case with finite methods if one only solved the marginal PDF's. Of course, such a procedure would be too heavy to implement. But this shows that the difficulty of finite methods does not come from their actual computational cost, but rather from their lack of versatility for discretizing composition spaces.

There exist generalizations of finite elements or volume methods which offer this versatility by treating part or the totality of the discretization in a Lagrangian or mesh-free

way. More generally, these methods belong to the class of particle and mesh-free methods (PMM's) [15,25,26], among which one finds the finite-point-set, SPH or PUM methods [15,25,26]. Such methods could be used as well to solve PDF equations or equivalent stochastic SPDE's. Thus, beyond the traditional Monte Carlo methods, there exists a whole spectrum of particle and mesh-free methods that could be readily applied or devised specifically to solve PDF equations.

As a conclusion, we would like to stress that all the mentioned methods aim at solving the same information. It is most likely that a difficulty encountered by one method will also be present in the other ones, even if under a different form. The choice of a method rather than another will then be a question of a compromise between the problems alleviated by a given method and its inherent difficulties.

VIII. CONCLUSIONS

A path is proposed to derive SPDE's allowing to compute the modeled one-point Fokker-Planck PDF of turbulent reactive scalars. A rapid decorrelating in time velocity field (Kraichnan [4], Kazantsev [5]) is used to model turbulent scalar advection. The initial Kr-Ka model is modified to account for the general case of compressible, inhomogeneous, low-Mach-number turbulent reactive flows, with molecular diffusion effects. The obtained SPDE's are shown to be hyperbolic advection-reaction equations and are dealt with in a generalized sense. They allow one to establish a connection between Eulerian and Lagrangian Monte Carlo approaches through the notion of stochastic characteristic.

The numerical integration of the SPDE's is discussed and a numerical scheme is adapted. Numerical tests are carried out on simplified one-dimensional configurations. Orders of accuracy and statistical convergence rates are checked and found to be conform with the theoretical ones, except for a symptomatic case which does not correspond to practical calculations.

The EMC method is currently applied to the calculation of a backward-facing step in combustion. Some results have already been obtained [17] and compared against experimental data. A qualitatively good agreement was found between mean temperatures and temperature variances. These promising results are now studied further and finer calculations are being carried out.

ACKNOWLEDGMENT

The authors would like to thank Professor S.B. Pope for useful comments on a preliminary draft of this article.

APPENDIX A: ELEMENTS OF PROOF

In this section, we first give the main steps leading to the derivation of the PDF equation of the scalar field θ, governed by SPDE (14). Then, by comparing this PDF equation to PDF equation (9), we obtain the constraint equations (15) and (16), which SPDE (14) must respect to be stochastically equivalent to PDF equation (9). Finally, as SPDE (19) satisfies those constraints, we deduce that SPDE (19) is stochastically equivalent to PDF equation (9).

For the sake of clarity, we introduce the following notations. First, we write the sum of the micromixing and chemical source terms present in SPDE (14) as a joint source term:

$$M(\theta;x,t)+S(\theta)=a_\theta(\theta,x,t)+\sqrt{2b_\theta(\theta,x,t)}\,\dot{W}. \tag{A1}$$

For the IEM model [Eq. (10)], we have

$$a_\theta=-\langle\omega_c\rangle(\theta-\tilde{\theta})+S(\theta),\quad b_\theta=0, \tag{A2}$$

and for the Langevin model [Eq. (11)],

$$a_\theta=-a\langle\omega_c\rangle(\theta-\tilde{\theta})+S(\theta),\quad b_\theta=b\langle\omega_c\rangle\theta(1-\theta). \tag{A3}$$

We also introduce the temporal increment of the velocity:

$$d\boldsymbol{v}=\tilde{\boldsymbol{U}}dt+\boldsymbol{u}dt=\tilde{\boldsymbol{U}}dt+\boldsymbol{u}^d dt+\boldsymbol{u}^g dt. \tag{A4}$$

With these notations, the material derivative of θ can be rewritten as

$$d\theta=a_\theta(\theta,x,t)dt+\sqrt{2b_\theta(\theta,x,t)}\,dW, \tag{A5}$$

where the notation $d\theta$ stands for the material derivative of θ:

$$d\theta=\frac{\partial\theta}{\partial t}dt+dv_j\circ\frac{\partial\theta}{\partial x_j}. \tag{A6}$$

The Stratonovitch interpretation is used for the stochastic advection term and the Ito interpretation is used in the stochastic source term. The Brownian processes W_j are chosen independent from the Brownian process W used in the Langevin model.

It will be assumed in the proof that $d\boldsymbol{v}$ is spatially Lipschitz. This assumption will be validated later by the final expression of $\boldsymbol{u}$ [Eqs. (A20) and (A21)]. Indeed, it will be seen that $\boldsymbol{u}$ is determined by the turbulent diffusion coefficient Γ_T, which is spatially Lipschitz.

Let us now introduce the fine-grained characteristic function of θ:

$$\psi_\theta(\lambda,x,t)=e^{i\lambda\theta(x,t)}. \tag{A7}$$

By definition, the mean of ψ_θ is the characteristic function of θ, Ψ_θ—that is to say, the Fourier transform f_θ of the PDF of θ:

$$\Psi_\theta(\lambda;x,t)=\langle\psi_\theta\rangle(\lambda;x,t)=\int e^{i\lambda\theta}f_\theta(\theta;x,t)d\theta. \tag{A8}$$

In the context of Eq. (A5), the mean of an arbitrary function depending of θ is equivalently defined through the PDF of θ or by considering that the function is averaged over an infinite number of realizations of the stochastic processes $d\boldsymbol{v}$ and dW. As these processes are independent, we have

$$\Psi_\theta=\langle\langle\psi_\theta\rangle_W\rangle_v=\langle\langle\psi_\theta\rangle_v\rangle_W, \tag{A9}$$

where $\langle\cdot\rangle_v$ ($\langle\cdot\rangle_W$) denotes averaging over the realizations of $\boldsymbol{v}$ (W).

By making use of the classical calculus rules for the Stratonovitch advection term and of the Ito calculus rules for the stochastic source term, one derives the following equation for the material derivative of $\psi_\theta(\lambda,x,t)$:

$$d\psi_\theta = \frac{\partial\psi_\theta}{\partial t}dt + dv_j \circ \frac{\partial\psi_\theta}{\partial x_j} = \frac{\partial\psi_\theta}{\partial\theta}d\theta + \frac{1}{2}\frac{\partial^2\psi_\theta}{\partial\theta^2}d\theta^2 = \lambda\psi_\theta a_\theta dt + i\lambda\psi_\theta\sqrt{2b_\theta}\,dW - \lambda^2\psi_\theta b_\theta dt. \tag{A10}$$

In the second line, the term $\frac{1}{2}b_\theta(\partial^2\psi_\theta/\partial\theta^2)d\theta^2$ comes from application of the Ito stochastic calculus (see [13]). In the third line, Eq. (A5) was used to express $d\theta$ and $d\theta^2$. Only terms of order dt were kept in the expression of $d\theta^2$.

Then, by taking the mean of Eq. (A10), one obtains an equation for the characteristic function Ψ_θ:

$$\frac{\partial\Psi_\theta}{\partial t}dt + \left\langle\left\langle dv_j \circ \frac{\partial\psi_\theta}{\partial x_j}\right\rangle_v\right\rangle_W = i\lambda\langle\psi_\theta a_\theta\rangle dt - \lambda^2\langle\psi_\theta b_\theta\rangle dt, \tag{A11}$$

where the no-correlation property of the Ito product has been used: $\langle\psi_\theta\sqrt{2b_\theta}\,dW\rangle_W = 0$.

From this point on, there only remains to express the mean value $\langle dv_j \circ \partial\psi_\theta/\partial x_j\rangle_v$. For this purpose, we shall make use of the Ito transformation (B7):

$$dv_j \circ \frac{\partial\psi_\theta}{\partial x_j} = dv_j\frac{\partial\psi_\theta}{\partial x_j} + \frac{1}{2}d\left(\frac{\partial\psi_\theta}{\partial x_j}\right)dv_j = dv_j\frac{\partial\psi_\theta}{\partial x_j} - \frac{\partial}{\partial x_j}\left(\frac{1}{2}dv_j dv_k\frac{\partial\psi_\theta}{\partial x_k}\right) + \frac{1}{2}dv_k\frac{\partial dv_j}{\partial x_j}\frac{\partial\psi_\theta}{\partial x_k}. \tag{A12}$$

Taking the mean over the realization of $\boldsymbol{v}$ yields

$$\left\langle dv_j \circ \frac{\partial\psi_\theta}{\partial x_j}\right\rangle_v = \langle dv_j\rangle\frac{\partial\langle\psi_\theta\rangle_v}{\partial x_j} - \frac{\partial}{\partial x_j}\left(\frac{1}{2}\langle dv_j dv_k\rangle\frac{\partial\langle\psi_\theta\rangle_v}{\partial x_k}\right) + \frac{1}{2}\left\langle dv_k\frac{\partial dv_j}{\partial x_j}\right\rangle\frac{\partial\langle\psi_\theta\rangle_v}{\partial x_k}, \tag{A13}$$

where again the no-correlation property of the Ito product has been used: $\langle dv_j\,\partial\psi_\theta/\partial x_j\rangle = \langle dv_j\rangle\partial\langle\psi_\theta\rangle_v/\partial x_j$.

By inserting this expression into Eq. (A11), the following equation is obtained for Ψ_θ:

$$\frac{\partial\Psi_\theta}{\partial t}dt + \left(\langle dv_j\rangle + \frac{1}{2}\left\langle dv_j\frac{\partial dv_k}{\partial x_k}\right\rangle\right)\frac{\partial\Psi_\theta}{\partial x_j} = \frac{\partial}{\partial x_j}\left(\frac{1}{2}\langle dv_j dv_k\rangle\frac{\partial\Psi_\theta}{\partial x_k}\right) + i\lambda\langle\psi_\theta a_\theta\rangle dt - \lambda^2\langle b_\theta\psi_\theta\rangle dt. \tag{A14}$$

Finally, by taking the inverse Fourier transform of Eq. (A14), the equation for the PDF of θ is obtained:

$$\frac{\partial f_\theta}{\partial t} + \left(\langle dv_j\rangle + \frac{1}{2}\left\langle dv_j\frac{\partial dv_k}{\partial x_k}\right\rangle\right)\frac{\partial f_\theta}{\partial x_j} = \frac{\partial}{\partial x_j}\left(\frac{1}{2}\langle dv_j dv_k\rangle\frac{\partial f_\theta}{\partial x_k}\right) - \frac{\partial}{\partial\theta}[a_\theta(\theta,x,t)f_\theta] + \frac{\partial^2}{\partial\theta^2}[b_\theta(\theta,x,t)f_\theta]. \tag{A15}$$

For this equation to be identical to Eq. (9), the following constraints must be satisfied:

$$\frac{1}{2}\langle dv_j dv_k\rangle = \Gamma_T\delta_{jk}dt, \tag{A16}$$

$$\langle dv_j\rangle + \frac{1}{2}\left\langle dv_j\frac{\partial dv_k}{\partial x_k}\right\rangle = \tilde{U}_j dt - \frac{1}{\langle\rho\rangle}\frac{\partial\langle\rho\rangle}{\partial x_j}\Gamma_T dt. \tag{A17}$$

By substituting the expression of $d\boldsymbol{v}$ [Eq. (A4)] into Eqs. (A16) and (A17), one obtains the following constraints on u^g and u^d [Eqs. (15) and (16) in Sec. III]:

$$\frac{1}{2}\langle u_i^g(x,t)u_j^g(x,t)\rangle dt = \Gamma_T\delta_{ij}, \tag{A18}$$

$$u_j^d = -\frac{1}{2}\left\langle\frac{\partial u_i^g}{\partial x_i}(x,t)u_j^g(x,t)\right\rangle dt - \frac{1}{\langle\rho\rangle}\frac{\partial\langle\rho\rangle}{\partial x_j}\Gamma_T. \tag{A19}$$

In SPDE (19), the following expressions for $\boldsymbol{u}^g$ and $\boldsymbol{u}^d$ are taken:

$$u_j^g = \sqrt{2\Gamma_T}\dot{W}_j, \tag{A20}$$

$$u_j^d = -\frac{1}{2}\frac{\partial\Gamma_T}{\partial x_j} - \frac{1}{\langle\rho\rangle}\frac{\partial\langle\rho\rangle}{\partial x_j}\Gamma_T. \tag{A21}$$

This choice allows us to respect the constraints (A18) and (A19). Besides, the definitions of u^d and u^g in SPDE (19) satisfy the Lipschitz continuity assumption on which the proof exposed above is based. Indeed, they are only determined by the smooth turbulent coefficient Γ_T. Thus, the PDF derived from equation of SPDE (19) is identical to PDF equation (9).

In this proof, no assumption on the smoothness and the differentiability of the stochastic scalar field has been made, so that Eq. (19) has a generalized sense and, in particular, is valid for discontinuous stochastic scalar fields.

APPENDIX B: ITO TRANSFORMATION

In Sec. III, Eq. (20) was said to be stochastically equivalent to Eq. (19) with Stratonovitch interpretation. In this section the correspondence between Ito and Stratonovitch interpretation is precised.

The conversion between SODE's with Stratonovitch interpretation and SODE's with Ito interpretation is well known and documented [13]. This transformation can actually be extended directly to SPDE's. Let us for instance consider the following advection equation:

$$\frac{\partial c}{\partial t} + \sqrt{2\Gamma}\frac{\partial c}{\partial x}\circ dW = 0, \tag{B1}$$

where $\Gamma = \Gamma(x,t)$. We recall that the symbol $\circ$ in the stochastic product denotes the Stratonovitch interpretation, while the

absence of symbol in the stochastic product denotes the Ito interpretation. We also recall that only the Stratonovitch interpretation preserves the advection meaning of the stochastic product. It is possible to recast this SPDE as an SODE at an arbitrary point x_0:

$$dc|_{x_0}(t) = -\sqrt{2\Gamma}\left.\frac{\partial c}{\partial x}\right|_{x_0} \circ dW. \tag{B2}$$

Despite its apparent simplicity, the transformation from Eq. (B1) to Eq. (B2) involves nontrivial mathematical derivations [8]. From there, it is possible to apply the classical Ito transformation [13]:

$$\begin{aligned} dc|_{x_0}(t) &= -\sqrt{2\Gamma}\left.\frac{\partial c}{\partial x}\right|_{x_0} dW(t) \\ &\quad + \frac{1}{2}\sqrt{2\Gamma}\left.\frac{\partial c}{\partial x}\right|_{x_0}\frac{\partial}{\partial c}\left(\sqrt{2\Gamma}\left.\frac{\partial c}{\partial x}\right|_{x_0}\right)dt \\ &= -\sqrt{2\Gamma}\left.\frac{\partial c}{\partial x}\right|_{x_0} dW(t) + \frac{1}{2}\sqrt{2\Gamma}\left.\frac{\partial}{\partial x}\left(\sqrt{2\Gamma}\frac{\partial c}{\partial x}\right)\right|_{x_0} dt. \end{aligned} \tag{B3}$$

The passage from the first to the second line comes from the equality

$$\left.\frac{\partial c}{\partial x}\right|_{x_0}\frac{\partial}{\partial c} = \left.\frac{\partial}{\partial x}\right|_{x_0}. \tag{B4}$$

The following SPDE with Ito interpretation is finally obtained:

$$\frac{\partial c}{\partial t} + \sqrt{2\Gamma}\frac{\partial c}{\partial x}\,dW(t) = \frac{1}{2}\sqrt{2\Gamma}\frac{\partial}{\partial x}\left(\sqrt{2\Gamma}\frac{\partial c}{\partial x}\right)dt. \tag{B5}$$

This equation is stochastically equivalent to the Stratonovitch equation (B1). By applying this transformation to Eq. (19) with Stratonovitch interpretation, one readily obtains Eq. (20) with Ito interpretation.

It is also possible to present the Ito transformation in a different way. Indeed, for any function X of time, the infinitesimal increment $X \circ dW$ can be approximated, by definition of the Stratonovitch calculus, by

$$\begin{aligned} X \circ dW &= X(t + dt/2)[W(t + dt) - W(t)] \\ &= \left(X(t) + \frac{1}{2}dX\right)[W(t + dt) - W(t)]. \end{aligned} \tag{B6}$$

From there, the following Ito Stratonovitch correspondence is obtained:

$$X \circ dW = X\,dW + \frac{1}{2}dX\,dW. \tag{B7}$$

This transformation is just another expression of the one presented at the beginning of this section. Indeed, by applying transformation (B7) to Eq. (B2), one obtains (after dropping the notation $|_{x0}$ for clarity)

$$\begin{aligned} dc &= -\sqrt{2\Gamma}\frac{\partial c}{\partial x}\,dW - \frac{1}{2}d\left(\sqrt{2\Gamma}\frac{\partial c}{\partial x}\right)dW \\ &= -\sqrt{2\Gamma}\frac{\partial c}{\partial x}\,dW - \frac{1}{2}\frac{\partial c}{\partial x}d(\sqrt{2\Gamma})dW - \frac{1}{2}\sqrt{2\Gamma}\frac{\partial dc}{\partial x}dW \\ &= -\sqrt{2\Gamma}\frac{\partial c}{\partial x}\,dW - \frac{1}{2}\frac{\partial c}{\partial x}\frac{d(\sqrt{2\Gamma})}{dt}dt\,dW \\ &\quad + \frac{1}{2}\sqrt{2\Gamma}\frac{\partial}{\partial x}\left(\sqrt{2\Gamma}\frac{\partial c}{\partial x}\right)dW^2. \end{aligned} \tag{B8}$$

By considering that dW is of order $dt^{1/2}$ and by neglecting the terms of order $>dt$, one recovers Eq. (B5).

APPENDIX C: CONNECTION BETWEEN EULERIAN AND LAGRANGIAN PDF's

To explicit further the connection between Eulerian and Lagrangian PDF's, let us introduce, as in [12], the Lagrangian joint PDF of position and composition conditional on the initial solution $f_L(\Theta, x; t|\xi)$ and its fine-grained PDF:

$$f'_L(\Theta, x; t|\xi) = \delta(\Theta - \theta^+(t|\xi))\,\delta(x - x^+(t|\xi)). \tag{C1}$$

By definition,

$$f_L(\Theta, x; t|\xi) = \langle f'_L(\Theta, x; t|\xi)\rangle. \tag{C2}$$

Similarly, let us introduce the Eulerian PDF of θ, $f_E(\Theta; x, t)$, and its fine-grained PDF:

$$f'_E(\Theta; x, t) = \delta(\Theta - \theta(x, t)). \tag{C3}$$

By definition,

$$f_E(\Theta; x, t) = \langle f'_E(\Theta; x, t)\rangle. \tag{C4}$$

The Eulerian and Lagrangian fine-grained PDF are related by

$$\begin{aligned} \int j^+ f'_L(\Theta, x; t|\xi)d\xi &= \int f'_L(\Theta, x; t|\xi(x^+))dx^+ \\ &= \int \delta(\Theta - \theta^+(x^+, t))\,\delta(x - x^+)dx^+ \\ &= \delta(\Theta - \theta(x, t)) = f'_E(\Theta; x, t). \end{aligned} \tag{C5}$$

The first equality is due to the relation $j^+ d\xi = dx^+$ and the third one to the sifting property of δ functions.

This first relation is essential for numerical applications, as it shows that to recover Eulerian statistics from a set of particles, the sums on the particle ensemble must be pondered by the Jacobian. For instance, to compute the Eulerian mean of θ from a set of N particles, one has to use the following formula:

$$\tilde{\theta} \approx \frac{\sum_{k=1}^{N} j^+_{(k)}\theta^+_{(k)}}{\sum_{k=1}^{N} j^+_{(k)}}. \tag{C6}$$

As for the Eulerian and Lagrangian PDF's, they are related by considering the following relation:

$$\int f_L'(\Theta,x;t|\xi)d\xi = \int \frac{1}{j^+} f_L'(\Theta,x;t|\xi) j^+ d\xi = \int \frac{1}{j^+(x^+,t)} \delta(\Theta - \theta^+(x^+,t))\,\delta(x - x^+)dx^+ \tag{C7}$$

$$= \frac{1}{j(x,t)} \delta(\Theta - \theta(x,t)). \tag{C8}$$

By taking the mean of the left- and right-hand sides of this equation, one finally obtains

$$\int f_L(\Theta,x;t|\xi)d\xi = \left\langle \frac{1}{j}|\Theta \right\rangle f_E(\Theta;x,t). \tag{C9}$$

[1] V. R. Kuznetsov and V. A. Sabel'nikov, *Turbulence and Combustion* (Hemisphere, London, 1990).
[2] S. B. Pope, Prog. Energy Combust. Sci. **27**, 119 (1985).
[3] L. Valiño, Flow, Turbul. Combust. **60**, 157 (1998).
[4] R. H. Kraichnan, Phys. Fluids **11**, 945 (1968).
[5] A. Kazantsev, Sov. Phys. JETP **26**, 1031 (1968).
[6] G. Falkovich, K. Gawedzki, and M. Vergassola, Rev. Mod. Phys. **73**, 913 (2001).
[7] V. Klyatskin, W. Woyczynski, and D. Gurarie, in *Stochastic Modelling in Physical Oceanography*, edited by Adler (Birkhauser, Boston, 1996).
[8] G. Eyink and J. Xin, Nonlinearity **15**, 551 (2002).
[9] J. Villermaux and J. Devillon, *Encyclopedia of Fluid Mechanics* (Gulf Pub. Co., West Orange, NJ, 1986), pp. 707–768.
[10] V. A. Sabel'nikov and M. Gorokhovski, in *Proceedings of the Second International Symposium on Turbulence and Shear FLow Phenomena*, edited by E.Lindborg, A.Joahnsson, J.Eaton, J.Humphrey, N.Kasagi, M.Leschziner, and M.Sommerfeld [Royal Institute of Technology (KTH), Stockholm, Sweden, 2001].
[11] O. Soulard, V. Sabel'nikov, and M. Gorokhovski, Int. J. Heat Fluid Flow **25**, 875 (2004).
[12] S. B. Pope, *Turbulent Flows* (Cambridge University Press, Cambridge, England, 2000).
[13] C. Gardiner, *Handbook of Stochastic Methods*, 2nd ed. (Springer, New York, 1985).
[14] E. Godlewski and P. Raviart, *Hyperbolic Systems of Conservation Laws* Mathmatiques et Applications (Ellipses, Paris, 1991).
[15] E. Onate, S. Idelsohn, O. Zienkiewicz, and R. Taylor, Int. J. Numer. Methods Eng. **39**, 3839 (1996).
[16] J. García-Palacios and F.J. Lázaro, Phys. Rev. B **58**, 14937 (1998).
[17] O. Soulard and V. Sabel'nikov (unpublished).
[18] S. B. Pope, Combust. Sci. Technol. **25**, 159 (1981).
[19] H. Osnes and H. Langtangen, SIAM J. Comput. **19**, 799 (1998).
[20] M. Werner and P. Drummond, J. Comput. Phys. **132**, 312 (1997).
[21] M. Jardak, C.-H. Su, and G. Karniadakis, J. Sci. Comput. **17**, 319 (2002).
[22] M. Muradoglu, S. B. Pope, and D. A. Caughey, J. Comput. Phys. **172**, 841 (2001).
[23] M. R. H. Sheikhi, T. G. Drodza, P. Givi, and S. B. Pope, Phys. Fluids **15**, 2321 (2003).
[24] J. Pozorski, M. Waclawczyk, and J. Minier, in *Turbulence, Heat and Mass Transfer*, edited by K. Hanjalic, Y. Nagano, and M. Tummers (Begell House, New York, 2003), pp. 157–164.
[25] S. Li and W. Liu, Appl. Mech. Rev. **55** (2002).
[26] *Meshfree Methods for Partial Differential Equations*, edited by M.Griebel and M.A.Schweitzer (Springer, Berlin, 2005).